Gas Phase Spectroscopy

(BL2B2, 3A2, 3B, 4B, 8A1)

(BL8B1)

Study on Dissociation Processes of Core-excited Methanol Using Auger Electron-Photoion Coincidence Measurements

Y. Senba [a], Y. Mishima [a], M. Morita [a], Y. Suto [a], T. Goya [a], H. Yoshida [a], T. Gejo [b], K. Mase [c] and A. Hiraya [a]

[a] *Department of Physical science, Hiroshima University, Higashi-Hiroshima 739-8526, Japan.*

[b] *UVSOR, Institute for Molecular science, Okazaki 444-8585, Japan*

[c] *Photon Factory, Institute of Materials Structure Science, Tsukuba 305-0801, Japan*

Photofragmentation processes of core-excited methanol (CH_3OH) have been investigated.[1, 2] Initial-excited-state dependence in partial ion yield was observed for several fragment ion. For instance, suppressions of OH^+ and COH^+ yields were observed only at O1s→3sa' excitation. Since core-excited molecules mainly dissociate via various Auger decay processes, Auger electron-photoion coincidence (AEPICO) measurements for C1s and O1s excited CD_3OH were performed.

Experiments were carried out at a soft X-ray beamline BL8B1. Experimental procedure was described elsewhere.[3] Briefly, a cylindrical-mirror type electron energy analyzer (CMA)[4] and a reflectron-type time-of-flight mass spectrometer (R-TOF)[5] were used for the coincidence measurements. Electrons and ions were extracted by an electrostatic field of 40 V/cm. In such an experimental condition, energy resolution (E/ΔE) of CMA was estimated to be ~40 and mass resolution (M/ΔM) of R-TOF ~45.

Figures 1 and 2 show the total ion yield spectra for C1s and O1s excitation regions, respectively. Observed peaks around 288 and 534 eV are assigned to C1s→3sa' and O1s→3sa', respectively.[1] AEPICO spectra were obtained for these excitations and some of them are shown in Figs. 3 and 4. The intensities of OH^+ (mass: 17) and COH^+ (mass: 29) for O1s→3sa' in Fig. 4 are very weak in comparison with those for C1s→3sa' in Fig.3. Moreover, even when we change the Auger electron energy, that is, final state energy (FSE), the intensities of OH^+ and COH^+ are still quite low in comparison with those of other fragments, for instance CD_3^+ and DCO^+. These results would suggest the ultra-fast dissociation of O-H bond for CD_3OH at O1s→3sa' excitation. The time scale of such dissociation is considered to be several femtoseconds and is comparable with that of Auger decay.

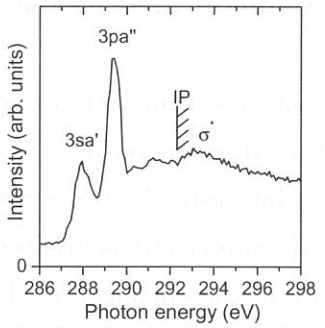

Fig.1. Total ion yield spectrum obtained for C1s excitation region.

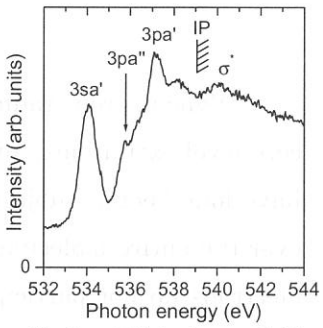

Fig.2. Total ion yield spectrum obtained for O1s excitation region.

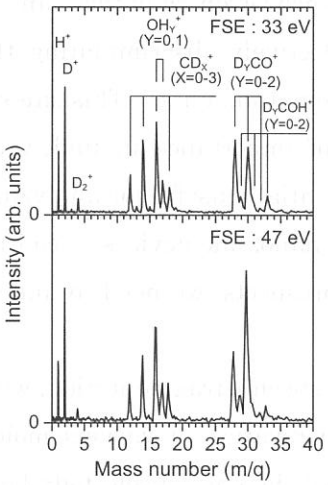

Fig.3. AEPICO spectra obtained for C1s→3sa'.

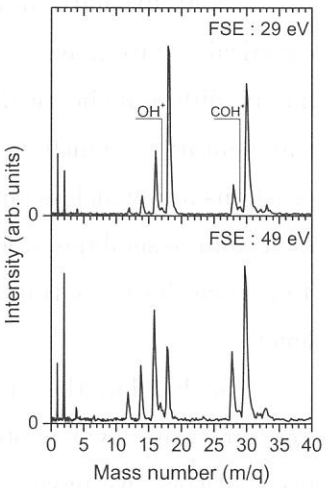

Fig.4. AEPICO spectra obtained for O1s→3sa'.

[1] A. Hempelmann et al., J. Phys. B: At. Mol. Opt. Phys., 32 (1999) 2677.

[2] T. Tokushima et al., SPing-8 User Experiment Report 7 (2001) 126.

[3] Y. Senba et al., to be published.

[4] T. Gejo et al., UVSOR Activity Report 1999, 27 (2000) 68.

[5] A. Hiraya et al., J. Electron Spectrosc. Relat. Phenom. 101-103 (1999) 1025.

(BL2B1)

Site-Specific Fragmentation Caused by N:1*s* Core-Level Photoionization of N_2O Condensed on a Si(100) Surface

Shin-ichi NAGAOKA, Akiko FUJII, Shin-ichiro TANAKA,[A] Kazuhiko MASE[B] and Kazutoshi TAKAHASHI[C]

Department of Chemistry, Faculty of Science, Ehime University, Matsuyama 790-8577

[A]Department of Physics, Graduate School of Science, Nagoya University, Chikusa-ku, Nagoya 464-8602

[B]Photon Factory, Institute of Materials Structure Science, High Energy Accelerator Research Organization, 1-1 Oho, Tsukuba 305-0801

[C]Institute for Molecular Science, Okazaki 444-8585

Synchrotron radiation has provided a powerful means to obtain information about core-level excitations, and the dynamic processes following the core-level excitations in molecules have long been a subject of interest. In contrast to valence electrons that are often delocalized over the entire molecule, the core electrons are localized near the atom of origin. Although core electrons do not participate in the chemical bonding, the energy of an atomic core-level in the molecule depends on the chemical environment around the atom. A shift in the energy levels of core electrons that is due to a specific chemical environment is called a chemical shift.

Monochromatized synchrotron radiation can excite core electrons of an atom in a specific chemical environment selectively, discriminating the core electrons from those of like atoms having different chemical environments. This site-specific excitation often results in site-specific fragmentation, which is of importance in understanding localization phenomena in chemical reactions and which is potentially useful for analyzing the structures and properties of molecules, molecular assemblies, and nanoscale devices by controlling matter at the level of individual atoms. To realize these exciting prospects, we need to understand what controls behavior at the atomic level.

To elucidate the site-specific fragmentation, we have studied the spectroscopy and dynamics following core-level photoionization of various molecules condensed on surfaces [1-5]. In the present work, we have used the energy-selected-photoelectron photoion coincidence (ESPEPICO) method to study the site-specific fragmentation caused by N:1*s* photoionization of N_2O condensed on a Si(100) surface. Since the chemical environment of the terminal N atom (N_t) is different from that of the central N atom (N_c), N_2O shows occurrence of different chemical shifts [6]. Thus N_2O may show site-specific fragmentation. The Si surface was cooled to about 50 K by flowing cold helium gas, and the sample was prepared by exposing the surface to N_2O gas at 10 L (1L = 1×10^{-6} Torr•s).

Figure 1 shows the photoelectron spectrum, which has two peaks in the region of N:1*s*

electron emission. The lower energy and higher energy peaks were respectively assigned to N_t:1*s* and N_c:1*s* electron emissions by comparison with the X-ray photoelectron spectrum obtained in the vapor phase [6]. The photoelectron spectrum thus clearly shows that the chemical shifts (binding energies) at the two nitrogen atoms are different.

Figure 2 shows the ESPEPICO spectra obtained with emission of the N_t:1*s* and N_c:1*s* electrons. N^+ (and/or O^+) and N_2O^+ ions are desorbed coincidentally with N:1*s* electrons. The site-specificity for these ions in N_2O condensed on a Si(100) surface is less remarkable than expected. The reason for this is thought to be that the two nitrogen sites are close to each other. In fact, we previously showed that site-specificity in $X_3Si(CH_2)_nSi(CH_3)_3$ (X=F or Cl, *n*=0-2) decreases with decreasing distance between the two silicon sites [3]. As in $X_3Si(CH_2)_nSi(CH_3)_3$, effective electron migration among the two nitrogen sites is probably responsible for the absence of site-specificity. Since the site specificity to a site adsorbed to a substrate is enhanced by electron transfer from the substrate to that site, we now attempt to perform the ESPEPICO experiments of N_2O adsorbed on a Si(100) surface.

References

[1] S. Nagaoka, K. Mase, M. Nagasono, S. Tanaka, T. Urisu and J. Ohshita, J. Chem. Phys. **107**, 10751 (1997).

[2] S. Nagaoka, K. Mase and I. Koyano, Trends Chem. Phys. **6**, 1 (1997).

[3] S. Nagaoka, K. Mase, M. Nagasono, S. Tanaka, T. Urisu, J. Ohshita and U. Nagashima, Chem. Phys. **249**, 15 (1999).

[4] K. Mase, S. Tanaka, S. Nagaoka and T. Urisu, Surf. Sci. **451**, 143 (2000).

[5] S. Nagaoka, S. Tanaka and K. Mase, J. Phys. Chem. B **105**, 1554 (2001).

[6] K. Siegbahn, C. Nordling, G. Johansson, J. Hedman, P. F. Hedén, K. Hamrin, U. Gelius, T. Bergmark, L. O. Werme, R. Manne, and Y. Baer, *ESCA Applied to Free Molecules* (North-Holland, Amsterdam, 1969).

Figure 1 (bottom). Photoelectron spectrum of N_2O taken at a photon energy of 442.5 eV.

Figure 2 (right-hand side). ESPEPICO spectra of N_2O taken at a photon energy of 467.2 eV. N_t:1*s* electron emission. (b) N_c:1*s* electron emission.

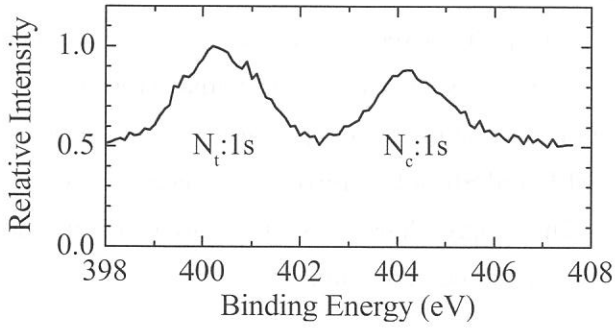

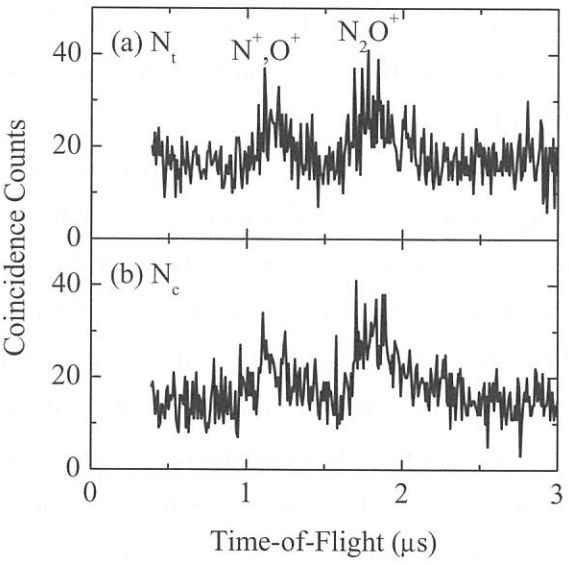

(BL3A1, BL7B)

Pump /Probe Experiments with FEL and SR Pulses at UVSOR

Tatsuo GEJO, Eiji SHIGEMASA, Eiken NAKAMURA, Masahito HOSAKA, Shigeru KODA, Akira MOCHIHASHI, Masahiro KATOH, Jun-ichiro YAMAZAKI, Kenji HAYASHI, Yoshifumi TAKASHIMA and Hiroyuki HAMA[a]

Institute for Molecular Science, Myodaiji, Okazaki 444-8585, Japan

[a]Laboratory of Nuclear Science, Tohoku University, Sendai 980 Japan

Introduction

Storage Ring Free Electron Laser (SRFEL or FEL) has been developed as a powerful light source owing to its high power, high coherence and unique temporal feature. Pump and probe experiments using FEL and synchrotron radiation (SR) pulses have been tried to perform for the last decade, because the FEL pulse naturally synchronizes with the SR one.

Very recently, as the first gas-phase experiment combined FEL with SR, we have carried out the two-photon double-resonant excitation on Xe atoms, utilizing a SR pulse as a pump and an FEL pulse as a probe light. Here we report the present status and future plan for the combined experiments with FEL and SR at UVSOR. The first experimental results on the two-photon double-resonant excitation of the Xe* $5p^5nf$ autoionization states using the combination of a mode-locked laser and SR have already been demonstrated by Meyer's group at LURE. In the present work, the combination of FEL and the undulator radiation was chosen in place of the former.

Experiments

The experiments were done on the undulator beamline BL3A1 and bending-maget-based beamline BL7B at UVSOR. At BL3A1, no monochromator is installed. Therefore, an LiF filter was employed to suppress higher order harmonics of the undulator radiation. The estimated photon flux of BL3A1 is about 1×10^{13} photons/sec/0.1%B.W at I = 100 mA and that of BL7B is in the order of 10^9.

The FEL pulses were extracted through the backward mirror and transported to experimental stations through a series of multi-layer mirrors. The flight path of FEL, which was adjusted to synchronize timing between the FEL and the SR pulses, was about 30 m. A focusing mirror (f = 10 m) was placed in the center of the flight path to keep the beam size of FEL small throughout the transport. About 69 % of the extracted power were transferred to the experimental station. Fine-tuning of the delay timing was made by using a movable optical delay system (50 cm) at the experimental station. The FEL and SR pulses introduced coaxially crossed an effusive jet of Xe atoms from a gas nozzle. The singly charged Xe ions produced in the interaction region were detected by means of a conventional channeltron.

Results and discussion

The fundamental harmonic of the undulator was adjusted to be 10.4 eV, in order to prepare the Xe* $5p^5 5d$ intermediate states as a first step. The Xe* $5p^5 4f$ autoionization resonance can be excited within the wavelength region of FEL as a second step. Because the lifetime of the intermediate states is quite short (600 ps), the synchronization between the SR and laser pulses is essential in this experiment.

During the experiment, there were serious background signals due to scattered stray light of SR pulses (typically about 10^5 counts/sec), which made it difficult to detect the real ion signals. Therefore, for searching the real signals, we temporarily employed the Q-switching technique. In this technique, much larger peak power of FEL is provided, although the duration of lasing becomes relatively short (~ 0.2 msec). However, if events are selected only during this duration, the improvement of signal to noise ratio (S/N) by a factor of 100 can be achieved.

After the precise alignment of the beams and the gas nozzle position by the Q-switching technique, we have measured the ion yield spectrum for the autoionization Xe* $5p^5 4f$ resonance using a CW FEL (Fig. 1). During the measurement, a newly developed feedback system was operated to stabilize the lasing. The asymmetric line shape described by the Fano formula has been clearly observed in Fig. 1.

In order to realize the angular distribution measurements of photoelectrons, considerable reduction of the background signals is necessary. Therefore we used the same experimental setup and performed the same measurement at BL7B, where a high-resolution monochromator is installed. The count rate for this measurement is about 200 counts/sec, which is about 1/1000 in comparison with the case when the undulator radiation was used. Figure 2 shows the two-photon ionization signals of Xe as a function of the wavelength of SR. Although the photon intensity of SR at BL7B is high enough to obtain total ion yield spectrum, it is not high enough to measure the angular distribution of photoelectrons.

We are planning to carry out similar experiments in the shorter wavelength region (around 400 nm) of FEL, where higher Rydberg series of the Xe* $5p^5 nf$ states via the Xe* $5p^5 5d$ intermediate state are accessible.

Reference [1] M. Gisselbrecht, A. Marquette and M. Meyer, J. Phys. B31 L977 (1998)

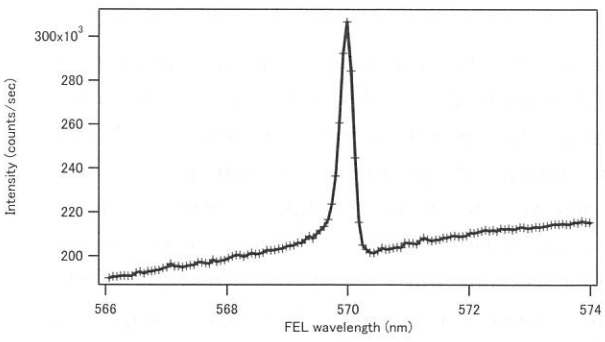

Fig. 1 Two-photon ionization signal of Xe as a function of the wavelength of FEL

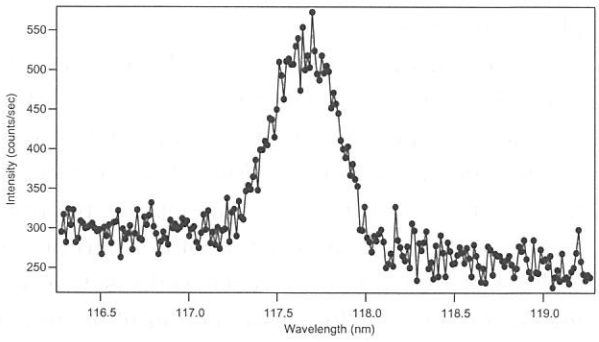

Fig. 2 Two-photon ionization signal of Xe as a function of the wavelength of SR

(BL3A2)

Molecular and Dissociative Single and Double Photoionization of CS_2 and Ionic Fragmentation of CS_2^+ and CS_2^{2+} in the Range from 20 to 120 eV

Toshio MASUOKA, Masahiro KATO, and Ataru KOBAYASHI

Department of Applied Physics, Graduate School of Engineering,, Osaka City University, Sugimoto 3, Sumiyoshi-ku, Osaka 558-8585

In order to study molecular and dissociative single and double photoionization and subsequent dissociation processes of CS_2, we have studied these processes with time-of-flight mass spectrometry and the photoion-photoion-coincidence (PIPICO) method by use of synchrotron radiation in the photon energy range of 20-120 eV. The TOF mass spectra and the PIPICO spectra were measured at an angle of ~55° with respect to the polarization vector where the second-order Legendre polynomial is close to zero. Under these conditions, the effects of anisotropic angular distributions of fragment ions are minimized. Appropriate optical filters (Sn and Al) were used to eliminate higher order radiation. To obtain accurate ion branching ratios, the radio frequency (rf) signal of the storage ring was used as the start signal of a time-to-amplitude converter (TAC) under the single bunch mode operation of the storage ring.

The present study focuses on the determination of the ratio of double to single photoionization (σ^{2+}/σ^{+}) as a function of photon energy. Second, the ion branching ratios for the individual ions produced from the parent CS_2^+ and CS_2^{2+} ions are separately determined. Third, the dissociation ratio of the parent CS_2^{2+} ions into two ionic fragments is determined. Some of the results are presented in this report.

Shown in Fig. 1 is a typical PIPICO spectrum measured at a photon energy of 72.5 eV. Only two dissociation channels of CS_2^{2+}, namely $S^+ + CS^+$ and $S^+ + C^+ + S$, are observed, whereas Lablanquie *et al.* [1] observed three dissociation channels $S^+ + C + S^+$ in addition to the above two channels. From the spectral profile of the coincident peaks, the discrimination against energetic ions is little, if any. The threshold of double ionization forming molecular CS_2^{2+} is at 27.0 ± 0.5 eV in good agreement with 27.05 ± 0.02 eV (the best previously reported value) measured by TPEsCO spectroscopy [2]. Metastable CS_2^{2+} ions are observed in the mass spectra. The ratio of double to single photoionization is shown in Fig. 2, increasing monotonically with photon energy. Since the $S^+ + C + S^+$ channel is not measured in the present experiments, the ratios in Fig. 2 should be regarded as representing a lower limit. Since the reliable total photoabsorption cross section of CS_2 in this wide photon energy range has not been reported, the σ^{2+}/σ^{+} ratios can not be converted to the absolute cross sections for single and double photoionization.

Ion branching ratios for the individual ions respectively produced from the parent CS_2^+ and CS_2^{2+} ions are determined separately, thus enabling more detailed study of the dissociation processes of the CS_2^+ and CS_2^{2+} ions. These results are shown in Figs. 3 and 4. Looking at the ion branching ratios of CS_2^+ (Fig. 3), we notice that the major ions produced are parent CS_2^+ and their ratios still increase at higher photon energies which suggests that electronic states contributing to the production of the parent CS_2^+ ion exist at these higher energies. Other details of Figs. 3 and 4 will be discussed elsewhere. Because we had some technical problems in the measurements of the ion-detection efficiency and the ion counting rates, which are essential to evaluate the σ^{2+}/σ^{+} ratios, the present results should be regarded as preliminary ones.

REFERENCES

[1] P. Lablanquie *et al.* JCP 82, 2951 (1985). [2] M. Hochlaf *et al.* CP 234, 249 (1998).

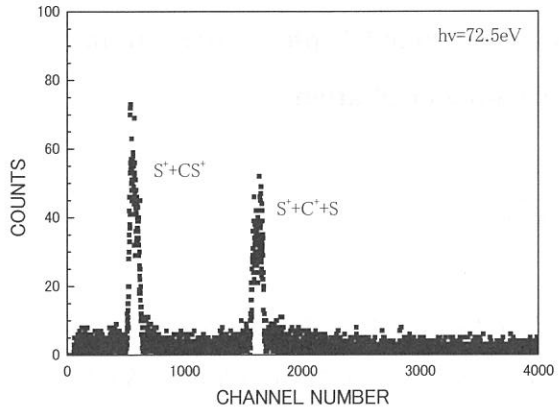

FIG. 1. A typical PIPICO spectrum measured at a photon energy of 72.5 eV.

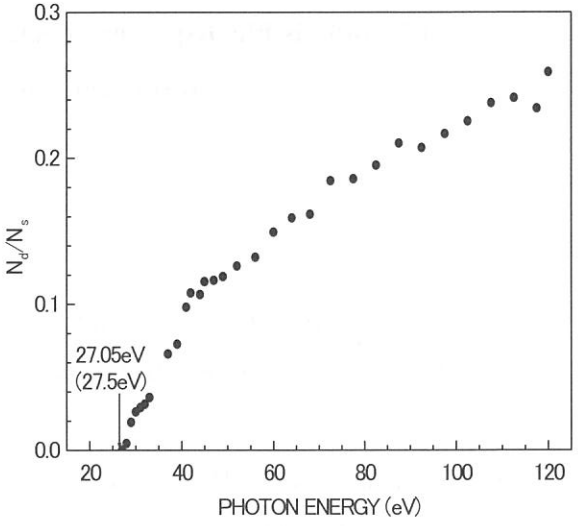

FIG. 2. Ratios of double to single photo-ionization cross section of CS_2.

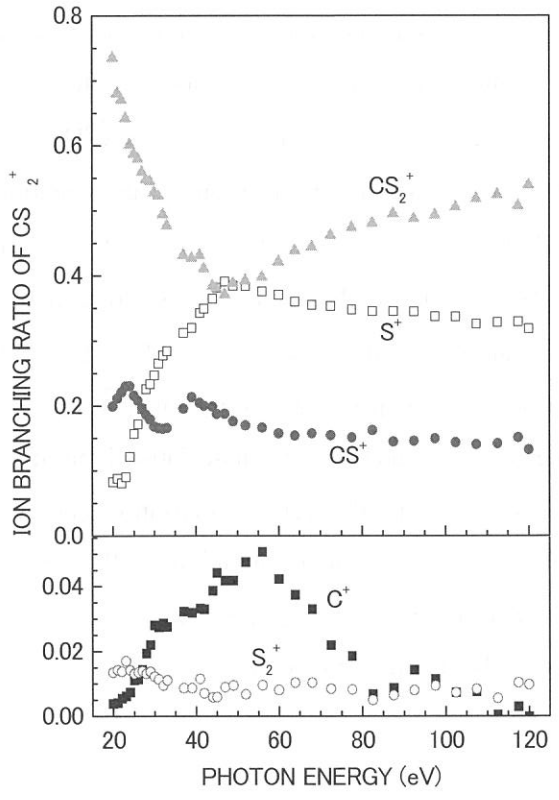

FIG. 3. Ion branching ratios of single photo-ionization of CS_2.

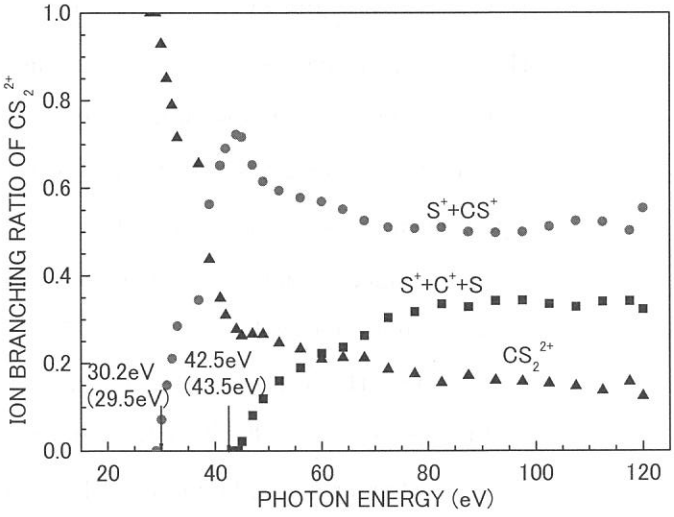

FIG. 4. Ion branching ratios of double photo-ionization of CS_2.

(BL3A2)

UV and visible dispersed spectra from the extreme UV photodissociation of the water using synchrotron radiation

Koichiro Mitsuke

Institute for Molecular Science, Myodaiji, Okazaki 444-8585, Japan

Department of Structural Molecular Science, The Graduate University for Advanced Studies

The photofragmentation of H_2O has been studied by fluorescence spectroscopy at photon energies between E_{hv} = 19.8 – 54.5 eV [1]. The primary photon beam was monochromatized undulator radiation supplied from the UVSOR synchrotron radiation facility. The fluorescence in the wavelength range of 280 – 720 nm was dispersed with an imaging spectrograph. The dispersed spectra in Figure 1 exhibit the hydrogen Balmer lines of $H^*[n\,^2L'_{J'} \rightarrow 2^2L''_{J''}(n=3-9)]$ and the emission band systems of $H_2O^+[\tilde{A}^2A_1(0,v'_2,0) \rightarrow \tilde{X}^2B_1(0,0,0)]$, $OH^+(\tilde{A}^3\Pi_\Omega, v' \rightarrow \tilde{X}^3\Sigma^-, v'')$, and $OH(\tilde{A}^2\Sigma^+, v' \rightarrow \tilde{X}^2\Pi_\Omega, v'')$. The fluorescence cross sections for these transitions have characteristic dependences on E_{hv} and vibrational quantum numbers. The cross section summed over the Balmer lines takes a minimum value at E_{hv} = 21.7 eV and steadily increases with increasing E_{hv} beyond 24.9 eV. This behavior is understood as that the superexcited states correlating with H*(n≥3) + OH($\tilde{A}^2\Sigma^+$) are too repulsive to be accessible at E_{hv} = 21.7 eV by the Franck-Condon transitions from $H_2O(\tilde{X}^1A_1)$. The appearance energy of the $OH^+(\tilde{A}^3\Pi_\Omega, v' \rightarrow \tilde{X}^3\Sigma^-, v'')$ transitions is found to be ca. 27 eV. This value is much higher than the dissociation limit of 21.5 eV for the $OH^+(\tilde{A}^3\Pi_\Omega)$ + H(n=1) channel, but agrees well with the vertical ionization energy to $H_2O^+[(1b_1)^{-2}(4a_1)^1\,^2A_1]$ that has been assumed to correlate with the above dissociation limit in the literature [2]. The vibrational distribution of $OH^+(\tilde{A}^3\Pi_\Omega)$ evaluated from the $OH^+(\tilde{A}^3\Pi_\Omega, v' \rightarrow \tilde{X}^3\Sigma^-, v'')$ band intensities is similar to the prior distribution in the rigid-rotor harmonic-oscillator approximation.

Reference

[1] K. Mitsuke, *J. Phys. B,* submitted.

[2] J. Appell and J. Durup, *Int. J. Mass Spectrom. Ion Phys.* **10**, 247 (1972/73).

Figure 1. Dispersed fluorescence spectra of H_2O encompassing the wavelength region 300 – 700 nm at six photon energies between E_{hv} = 19.8 and 43.5 eV. The $2_0^{v'}$ symbols in the panel of E_{hv} = 19.8 eV designate the vibrational progression in the bending mode ν_2 of the $H_2O^+[\tilde{A}^2A_1(0,v'_2,0) \rightarrow \tilde{X}^2B_1(0,0,0)]$ transition. The hydrogen Balmer lines $H^*[n\,^2L'_{J'} \rightarrow 2^2L''_{J''}(n=3-9)]$ are indicated by the (n→2) marks.

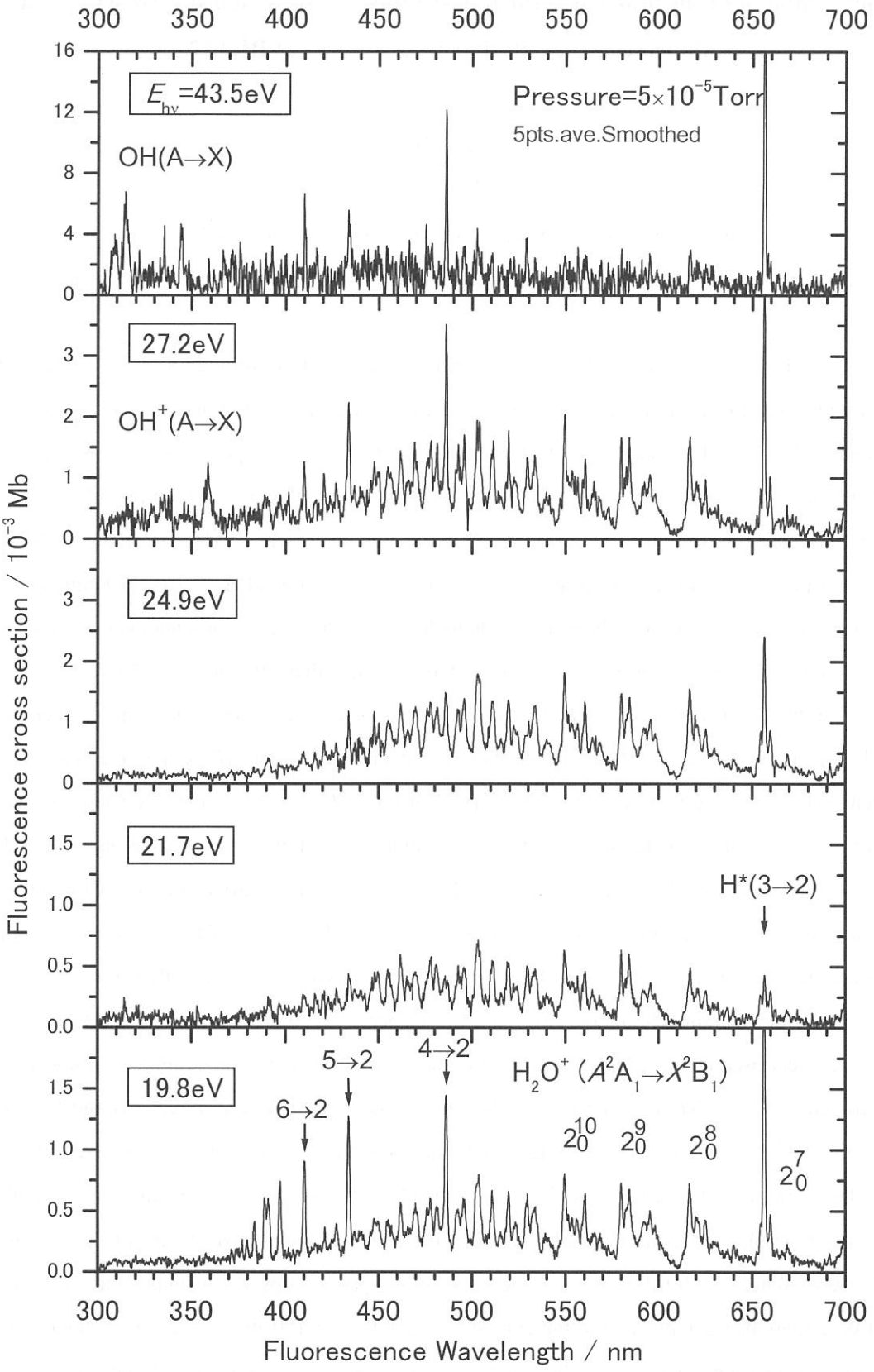
$E_{h\nu}$=43.5eV
Pressure=5×10^{-5}Torr
5pts.ave.Smoothed
OH(A→X)
27.2eV
OH$^+$(A→X)
24.9eV
21.7eV
H*(3→2)
19.8eV
6→2
5→2
4→2
H$_2$O$^+$ (A^2A$_1$→X^2B$_1$)
2_0^{10}
2_0^9
2_0^8
2_0^7
Fluorescence cross section / 10^{-3} Mb
Fluorescence Wavelength / nm

(BL3A2)

Development of the apparatus for high-resolution dispersed spectroscopy and fluorescence excitation spectroscopy at BL3A2

Koichiro Mitsuke

Institute for Molecular Science, Myodaiji, Okazaki 444-8585, Japan
Department of Structural Molecular Science, The Graduate University for Advanced Studies

The sample gas was expanded under an effusive jet condition through a multichannel capillary plate, and subjected to the irradiation of monochromatized undulator radiation (E_{hv}= 15 – 55 eV). The fundamental light or its third harmonic of the undulator radiation was dispersed by a monochromator of constant deviation grazing-incidence type with a 2.2 m focal length. A typical photon intensity and spectral resolution of the synchrotron radiation were $(2 – 8) \times 10^{14}$ photons s^{-1} cm^{-2} and 2.4 Å (FWHM, 83 meV at 20.85 eV), respectively, with entrance- and exit-slit widths of 300 μm. There exists contamination of the light by passage of a second order through the monochromator from the second undulator harmonic. The concentration of the second-order light was estimated to be no less than 10% at E_{hv} = 15 eV.

The fluorescence was collected by an optical detection device in Fig. 1 made up of spheroidal and spherical mirrors facing each other across the photoexcitation region (*PR*), i.e. the source of the fluorescence [1]. One focal point of the spheroidal mirror fell at *PR*, while the other focal point was at the surface of an optical-fiber bundle of 45 cm long. The fluorescence light was reflected back to *PR* by the spherical mirror with its focal point at *PR*, and was then focused onto the surface of the fiber bundle by the spheroidal mirror. This detection system can collect light from about 62% of the full-sphere solid angle. The fluorescence passed through the optical-fiber bundle (transmission ~ 55% at 400 nm).

Two types of monochromators were used to disperse the fluorescence (*e.g.* Fig.2). In dispersed fluorescence spectroscopy we utilized a 300 mm focal-length imaging spectrograph equipped with a liquid-nitrogen cooled CCD array detector of 26.8 mm wide (the dispersion direction) and 8 mm high. Normally 600 and 1200 grooves/mm gratings having nominal blaze wavelengths of 300 and 500 nm were chosen. The overall detection efficiency, including the spheroidal and spherical mirrors, fiber bundle, and imaging spectrograph, was estimated to be $(1 - 5)\times10^{-3}$ with the entrance slit width of the spectrograph being 250 μm. When we fulfilled fluorescence excitation spectroscopy by scanning the wavelength of synchrotron radiation, we replaced the imaging spectrograph by a 100 mm focal-length monochromator and a photomultiplier tube. In this case, the overall detection efficiency was estimated to be $(1.4 \pm 0.3)\times10^{-3}$ at the entrance- and exit-slit widths of the monochromator of 2 mm. All spectra were corrected by the wavelength dependence of the relative detection efficiency.

Reference

[1] K. Mitsuke and M. Mizutani, *Bull. Chem. Soc. Jpn.* **74**, 1193 (2001).

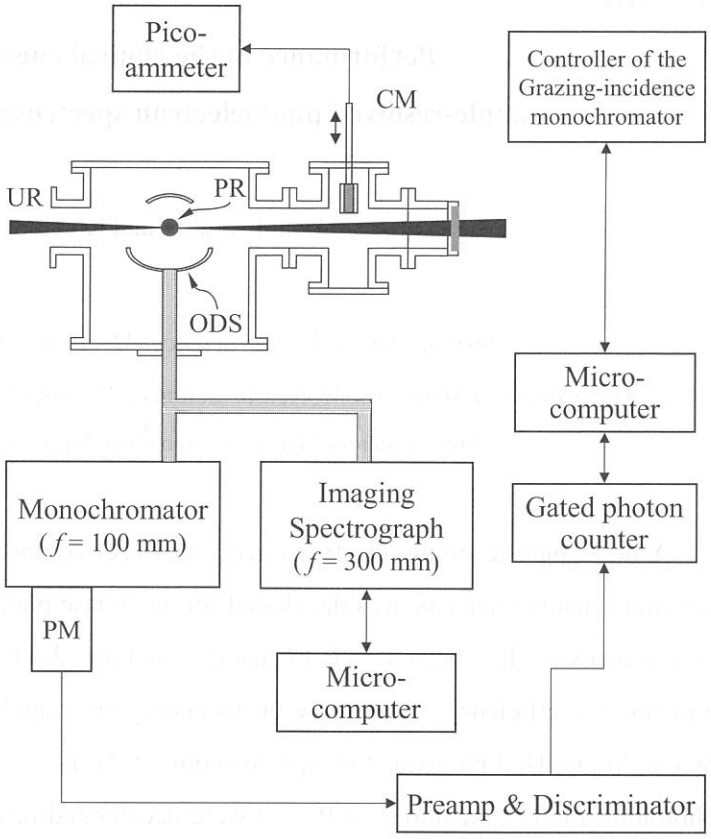

Fig. 1. Schematic diagram of the apparatus for dispersed fluorescence spectroscopy and fluorescence excitation spectroscopy. UR, monochromatized undulator radiation; PR photoexcitation region (not to scale); ODS, optical detection system composed of spheroidal and spherical mirrors and an optical-fiber bundle; CM, gold-mesh current monitor; PM, photomultiplier.

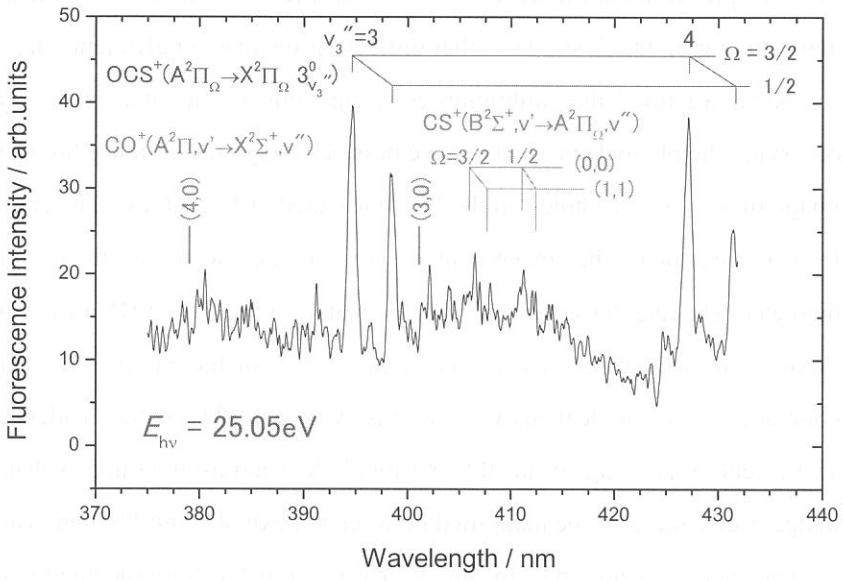

Fig. 2. Dispersed fluorescence spectra of OCS encompassing the wavelength region 375 – 431 nm at E_{hv} = 25.05 eV. The spectrum was measured by using the imaging spectrograph equipped with a 1200 grooves/mm grating which has a nominal blaze wavelength of 300 nm. The entrance-slit width was set to 250 μm. The thin short vertical lines indicate two spin-orbit components (Ω = 3/2 and 1/2) of the vibrational bands of the $OCS^+[A^2\Pi_\Omega(0,0,0) \rightarrow X^2\Pi_\Omega(0,0,v_3'')]$ transition with $v_3'' = 3$ and 4. The thin long vertical lines indicate the two spin-orbit components of the vibrational bands of the $CS^+(B^2\Sigma^+,v' \rightarrow A^2\Pi_\Omega,v'')$ transition. The (v',v'') mark denotes the band due to the transition from the upper v' to lower v'' vibrational states. The thick vertical lines indicate the band origins of the $CO^+(A^2\Pi_\Omega,\ v' \rightarrow X^2\Sigma^+,\ v''=0)$ emission-band system.

(BL3B)

Performance of the conical energy analyzer for angle-resolved photoelectron spectroscopy developed at BL3B

Kota Iwasaki [a] and Koichiro Mitsuke

Institute for Molecular Science, Myodaiji, Okazaki 444-8585, Japan

Department of Structural Molecular Science, The Graduate University for Advanced Studies

[a] Present address: Shimadzu corporation, Nakagyo-ku, Kyoto 604-8511, Japan

A new angle-resolving electron energy analyzer composed of a conical electrostatic prism and a position sensitive detector was developed for gas-phase photoelectron spectroscopy. The performance of the analyzer has been tested by using a helium discharge lamp. Namely, we have tested the transmission efficiency of the analyzer, its energy and angular resolutions, and background count rate by employing He I photoelectron spectroscopy of Ar atoms. The 5.3 and 5.5eV electrons produced by photoionization of Ar into $Ar^+(^2P_{3/2,1/2})$ were decelerated or accelerated and made to pass through the analyzer. Since the light is unpolarized, the nascent photoelectron angular distribution is expected to be isotropic. Indeed, the observed electron intensity was almost constant over the whole range of the azimuth angle, which suggests that uniform transmission efficiency has been realized.

Next, we fitted the calibration cone electrode in the analyzer to evaluate the angular resolution by observing the photoelectrons that have passed through the entrance holes. Figure 1 shows a typical electron image of the entrance holes on the PSD measured at E = 5.6 eV. The angular resolution can be determined from the extent of the image. Three spots correspond to the three entrance holes of 1.5 and 2mm in diameter. The angular resolution was estimated to be 3° (FWHM) from the spot size for the 1.5mm hole. Taking into account the acceptance angle of 5.4° of the entrance hole from the sample volume, we can conclude that our conical analyzer has a converging effect on the incident electrons in the azimuth direction. The extent of the image of the 0.5 or 1 mm hole is almost the same as that of the 1.5 mm hole. The electron image is considered to be magnified between the exit slot and PSD unit owing to the fringing-field effect.

The energy resolution of the analyzer was estimated from the band-width of the $Ar^+(^2P_{3/2,1/2})$ peaks in a photoelectron spectrum. The spectrum was obtained by plotting the total electron counts within the image of the entrance hole of ϕ2 mm on the PSD, as a function of the potential difference between the gas cell and inner cone electrode. Figure 2 shows the photoelectron spectrum thus measured. The $Ar^+(^2P_{3/2,1/2})$ bands have symmetric Gaussian profile. It is thus likely that there exists no distortion in the electric field acting upon the photoelectrons from the gas cell. The signal to background ratio was found to be 10 - 20.

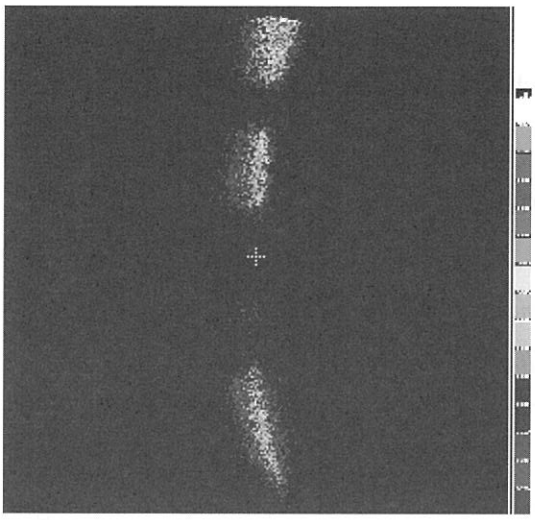

Fig. 1. Photoelectron image on the PSD. Three spots represent the image of three entrance holes bored through the inner cone electrode. The top spot is truncated along the edge of the PSD.

The minimum band-width of 60±1 meV (FWHM) has been achieved at E = 1.4 eV, i.e. the best energy resolution of $\Delta E/E$ = 0.043. This value amounts to 130 % of the resolution expected from our simulation of the electron trajectories. This deterioration can be explained by the assumption that we cannot optimize the deceleration voltages applied to the annular lens system yet. Conceivably, the lens system extracts superfluous electrons with large incident angles with respect to the mean trajectory in the dispersion plane under the present experimental conditions.

Reference

[1] K. Iwasaki and K. Mitsuke, *Surf. Rev. Letters,* in press.

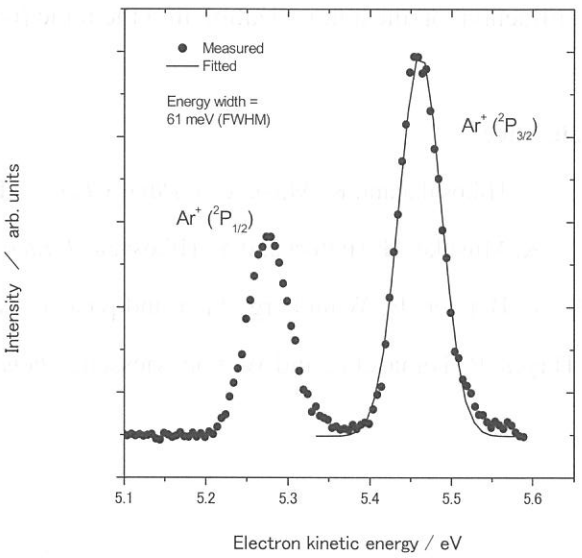

Fig. 2. He photoelectron spectrum of Ar. Two peaks are attributed to the $Ar^{+}(^{2}P_{2/3,1/2})$ bands. The ratio of the peak intensities is two and agrees with that of their statistical weights.

(BL3B)

Formation and autoionization of a dipole-forbidden superexcited state of CS_2

Yasumasa Hikosaka [a] and Koichiro Mitsuke [b]

[a] *Photon Factory, Institute of Materials Structure Science, 1-1 Oho, Tsukuba, 305-0801, Japan*

[b] *Institute for Molecular Science, Myodaiji, Okazkai 444-8585, Japan*

Department of Structural Molecular Science, The Graduate University for Advanced Studies

We have measured 2D-PESs of CS_2 in the $E_{h\nu}$ region of 14.60 - 15.35 eV, in order to investigate excitation and decay mechanisms of superexcited states [1,2]. The 2D-PESs show pronounced formation of the (0,0,1) levels of $CS_2^+(\tilde{X}\,^2\Pi_g$ and $\tilde{B}\,^2\Sigma_u^+)$ from a superexcited state at $E_{h\nu}$ = 14.88 eV. This unusual vibrational excitation of ions in the ν_3 mode results from autoionization of the (0,0,1) level of the dipole-forbidden state which has been assigned to the $3d\sigma_g$ $CS_2^*(R_C)$ state conversing to $CS_2^+(\tilde{C}\,^2\Sigma_g^+)$. The primary photoexcitation to the (0,0,1) level of the $3d\sigma_g$ state is considered to become allowed by vibronic interaction with the $5p\sigma_u$ $CS_2^*(R_C)$ state. We have additionally uncovered that the preference in autoionization of the $3d\sigma_g$ state into the final ionic states depends on their vibrational levels. The preference concerning the ionic (0,0,0) levels is explained in terms of the vibronic interaction that remains until autoionization, while the vibronic interaction is relatively uninfluential on the autoionization into the ionic (0,0,1) levels.

Reference

[1] Y. Hikosaka and K. Mitsuke, *J. Phys. Chem. A* **105,** 8130 (2001).

[2] K. Mitsuke, H. Hattori and Y. Hikosaka, *J. Electron Spectrosc. Relat. Phenom.* **112**, 137 (2000).

[3] P. Baltzer, B. Wannberg, M. Lundqvist, L. Karlsson, D.M.P. Holland, M.A. MacDonald, M.A. Hayes, P. Tomasello, and W. von Niessen, *Chem Phys.* **202,** 185 (1996).

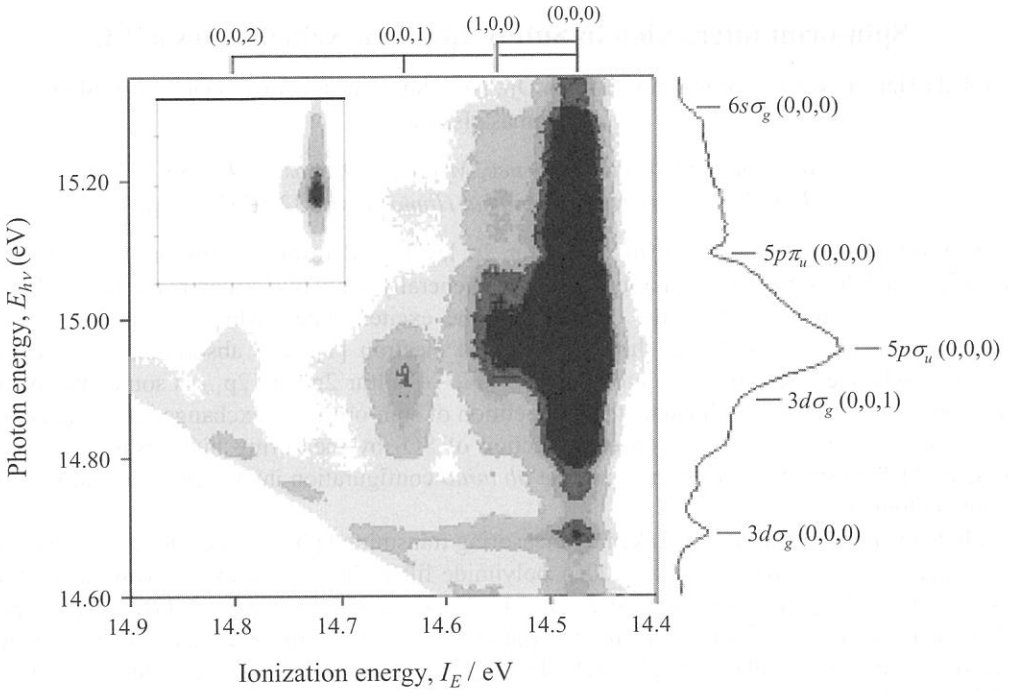

Fig. 1. Two-dimensional photoelectron spectrum for the $CS_2^+(\tilde{B}\ ^2\Sigma_u^+)$ band and its vicinities measured in the photon energy range of 14.60 - 15.35 eV. The electron yield is presented as a function of both photon energy $E_{h\nu}$ and ionization energy I_E by the plots with eight tones from light to dark on a linear scale. The curve in the right panel shows a constant ionic state spectrum, which is obtained by summing electron counts along the I_E axis at each $E_{h\nu}$. Five resonances of Rydberg states converging to $CS_2^+(\tilde{C}\ ^2\Sigma_g^+)$ are observed at $E_{h\nu}$ = 14.69, 14.88, 14.95, 15.09, and 15.31 eV. The former two states are first assigned in this work.

Fig. 2. One-dimensional photoelectron spectrum for the $CS_2^+(\tilde{B}\ ^2\Sigma_u^+)$ band, which is obtained by summing electron counts in Fig. 1 at every I_E over the $E_{h\nu}$ = 14.80 - 14.95 eV range along the $E_{h\nu}$ direction. Vibrational levels are indicated at the I_E positions reported in Ref. [3].

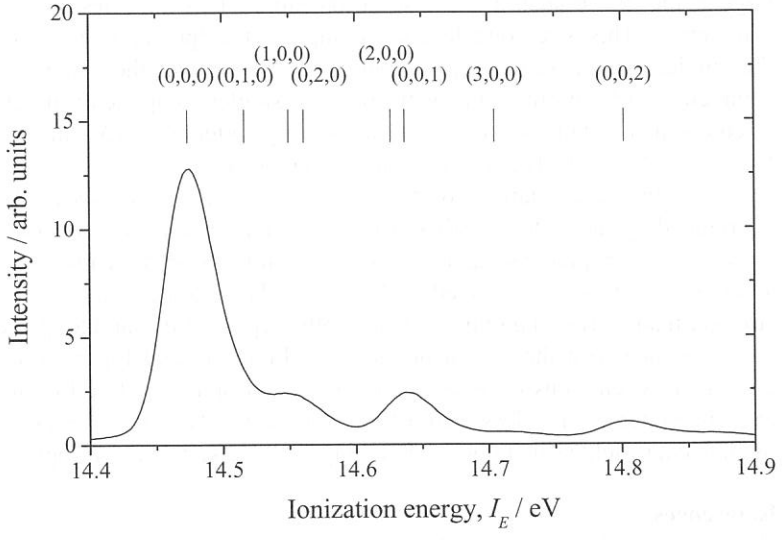

(BL4B)

Spin-orbit interaction in Sulfur 2p photoexcited states of SO_2

Takaki Hatsui, Mitsuru Nagasono, Hiroshi Oji, Nobuhiro Kosugi, Tatsuo Gejo, Eiji Shigemasa
Toshimasa Ishida*

Institute for Molecular Science, Myodaiji, Okazaki 444-8585
** Shizuoka University, Hamamatsu, Hamamatsu 432-8561, Japan*

Spin-orbit interaction is large in the sulfur 2p levels and resulting spin-orbit-split levels are well described as $2p_{3/2}$ and $2p_{1/2}$. Sulfur 2p photoexcited states generally show two structures separated by ~1 eV. The separation is, however, dependent on the character of the excited states, which can be explained by large exchange interaction between sulfur 2p hole and excited electron [1]. The absorption cross-section is also affected by the exchange interaction; the cross-section ratio of sulfur $2p_{3/2}$ to $2p_{1/2}$ is sometimes deviated from statistical value of 2:1. In order to elucidate the competition of spin-orbit and exchange interactions in detail, we have investigated anisotropy of absorption cross-section of SO_2 by measuring high-resolution angle-resolved photoion yield (ARPIS) spectra, and by carrying out *ab initio* configuration interaction calculations based on the Breit-Pauli hamiltonian.

Photoabsorption spectra were taken by measuring transmitted photon intensity using a Si diode. A few Torr SO_2 gas pressure was separated by a 1200 Å polyimide filter. Photon energy was calibrated by measuring Ar $2p_{3/2}$-4s* and Kr $3d_{3/2}$-5p absorption peaks at 244.4 and 92.425 eV, respectively. ARPIS spectra were measured by using two channeltron set in the 0° (parallel) and 90° (perpendicular) directions relative to the electric vector of the linearly polarized light. Retardation grids were used to detect energetic photoions (>3 eV). Ab initio MO calculations were performed using the GSCF3 code.

Figure 1 shows high-resolution photoabsorption and ARPIS spectra. In this report, we focus on excitations to π^* (b_1), σ^* (a_1), σ^* (b_2), and 4s (a_1). Figure 2 shows a part of ARPIS spectra of SO_2, where I_0 (I_{90}) corresponds to ion yields in the direction parallel (perpendicular) to the electric vector of the linear polarized incident light. This region includes only the S 2p excitation to the lowest unoccupied orbital of $\pi^*(b_1)$ symmetry. The S 2p orbitals have a_1, b_2 and b_1 symmetries, resulting in three S 2p-$\pi^*(b_1)$ excited states of B_1, A_2, and A_1 symmetries. The ground state symmetry is A_1 and the $A_2 \leftarrow A_1$ excitation is dipole-forbidden; that is, the $a_1 \rightarrow b_1^*(B_1)$ and $b_1 \rightarrow b_1^*(A_1)$ excitations should be observed in Figure 2. Theoretical calculations predicts that $a_1 \rightarrow b_1^*(B_1)$ and $b_1 \rightarrow b_1^*(A_1)$ excitations have nearly the same oscillator strengths (Table 1a). Considering the spin-orbit interaction, each singlet excitation is mixed with two triplet excitations, resulting in three excited states in each symmetry. The transition dipoles to the B_1 states are orthogonal to the molecular plane and these transitions give only I_{90} yields; on the other hand, the transitions to the A_1 states give both I_0 and I_{90} yields. In Figure 2, three electronic states of B_1 symmetry show vibrational fine structures, where the lowest electronic state is very weak, and the second ($^2P_{3/2}$) is stronger than the third ($^2P_{1/2}$). On the other hand, only two electronic states of A_1 symmetry appears in Figure 2, where one is located in the $^2P_{3/2}$ manifold, and the other is in the $^2P_{1/2}$ manifold. The $^2P_{1/2}$ feature seems to be slightly stronger that the $^2P_{3/2}$ feature, though the $^2P_{3/2}$ branch is as twice large as the $^2P_{1/2}$ branch in the case of ionization. This indicates that exchange interaction is essential in the A_1 symmetry. This is reasonable, considering that the $2p(b_1)$ and $\pi^*(b_1)$ orbitals are oriented parallel. Furthermore, the singlet excited state is quite higher in energy than the triplet excited state, and the lowest state of A_1 symmetry hardly borrows intensity from the singlet component; therefore, the lowest state is almost invisible. Theoretical calculations shows that the exchange interaction (Δ_{ST} in Figure 3a) in A_1 symmetry (1.5 eV) is much larger than Δ_{ST} in the B_1, and B_2 symmetries (<0.2 eV).

In the excitation to σ^* (a_1), broad bands were observed. Since the S $2p_{1/2}$-$\sigma^*(a_1)$ excitation is overlapped by the S $2p_{3/2}$-$\sigma^*(b_2)$, it is not straightforward to extract anisotropy information of each excitation. However, theory predicts that oscillator strength for S 2p-$\sigma^*(a_1)$ is dominated by $b_1 \rightarrow a_1^*(B_1 \leftarrow A_1)$ as in Table 1b. Thus, S $2p_{1/2}$-$\sigma^*(b_2)$ is expected to show the polarization dependence similar to S $2p_{3/2}$-$\sigma^*(b_2)$, where I_{90} yield is stronger than I_0. Based on this analysis, both S $2p_{3/2}$-$\sigma^*(b_2)$, and S $2p_{1/2}$-$\sigma^*(b_2)$ excitations show $I_0 > I_{90}$, which is in accordance with theoretical predictions (Table 1c, and Figure 3c). In Figure 1, both S $2p_{3/2}$-$4s(a_1)$, and S $2p_{1/2}$-$4s(a_1)$ excitations were revealed to be anisotropic ($I_0 > I_{90}$). Because of the Rydberg character of 4s orbital, exchange interaction is less than 0.1 eV (Figure 3d). Oscillator strengths, however, are rather strongly perturbed by molecular field as in Table 1d, resulting in the observed anisotropy.

References

[1] N. Kosugi, R.G. Cavell, A.P. Hitchcock, Chem. Phys. Lett., 265 (1997) 490.

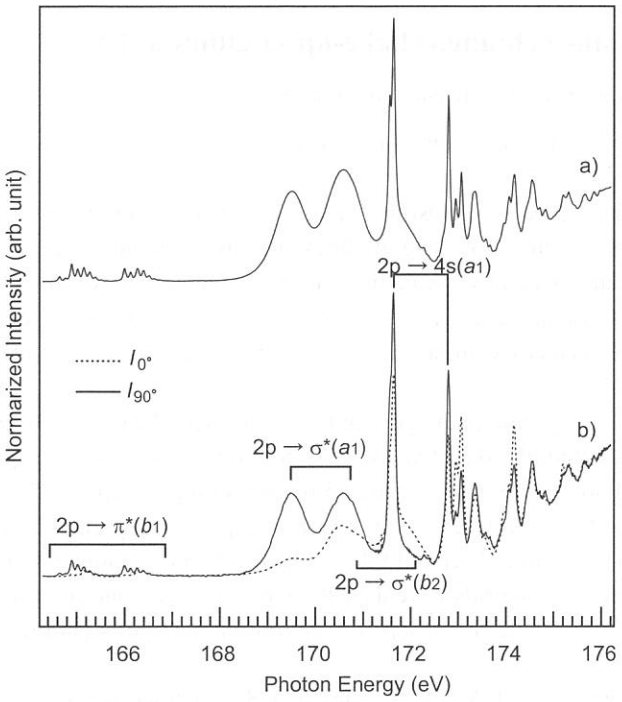

Figure 1. Sulfur 2p photoabsorption spectrum (a) and angle-resolved photoion-yield spectra for SO_2.

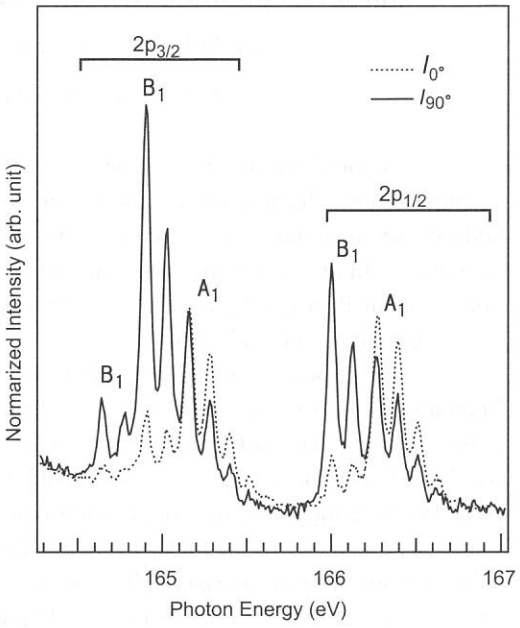

Figure 2. Angle-resolved ion-yield spectra for sulfur 2p→π* (b_1) transition.

Table 1. Theoretical osillator strengths for non-relativistic excited states.

(a) 2p → π*(b1)	Osillator strength for singlet
B1 [2pz (a1) → b1]	f=0.0016
A1 [2px (b1) → b1]	f=0.0016
A2 [2py (b2) → b1]	forbidden

(b) 2p → σ*(a1)	Osillator strength for singlet
A1 [2pz (a1) → a1]	f=0.0003
B1 [2px (b1) → a1]	f=0.0319
B2 [2py (b2) → a1]	f=0.0016

(c) 2p → σ*(b2)	Osillator strength for singlet
B2 [2pz (a1) → b2]	f=0.0124
A2 [2px (b1) → b2]	forbidden
A1 [2py (b2) → b2]	f=0.0127

(d) 2p → 4s*(a1)	Osillator strength for singlet
A1 [2pz (a1) → a1]	f=0.0016
B1 [2px (b1) → a1]	f=0.0050
B2 [2py (b2) → a1]	f=0.0016

Figure 3. Theoretically obtained correlation diagram of relativistic and non-relativistic states. Singlet states and it's perturbed states are indicated by thick lines. Percentages of each non-relativistic singlet component in relativistic states are indicated. Dipole forbidden states are omitted for clarity.

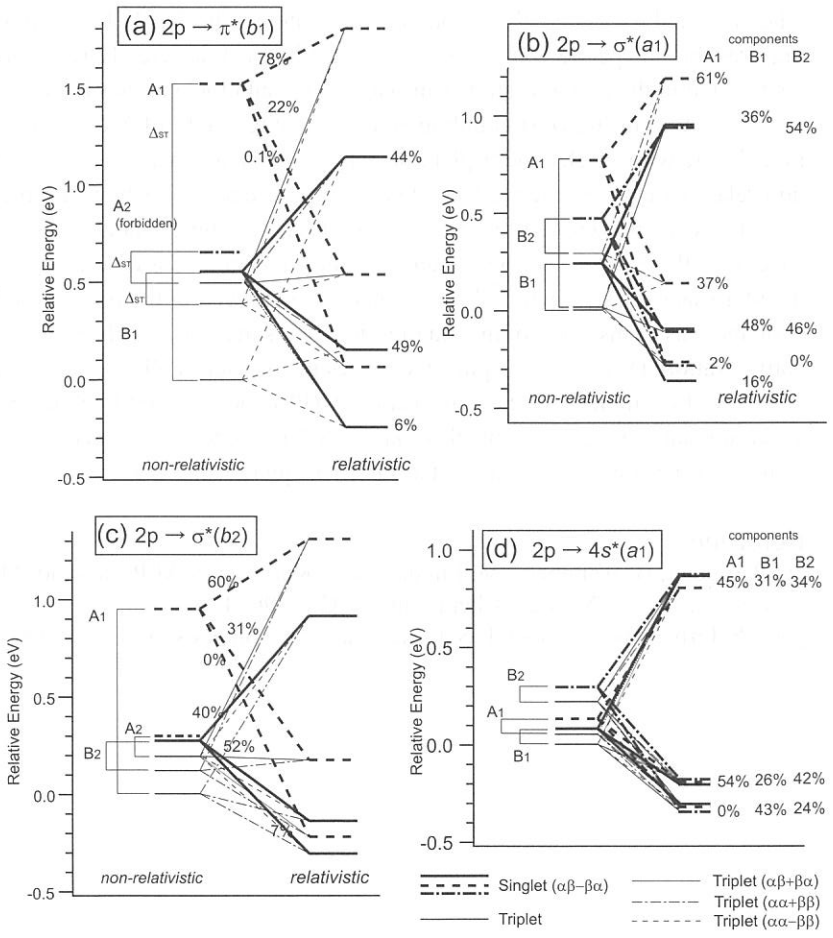

(BL4B)

Sulfur 2p photoexcited states and spin-forbidden shake-up satellites of CS_2

Takaki Hatsui , Mitsuru Nagasono, Eiji Shigemasa, Nobuhiro Kosugi

Institute for Molecular Science, Myodaiji, Okazaki 444-8585

Photoelectron spectroscopy (PES) is widely used to investigate the one-electron energy level in various matters. Because of electron correlation effect, spectra show satellite lines such as shake-up satellites in addition to main lines. These correlation satellites are generally weak but can be enhanced by exciting at resonances. In this report we for the first time demonstrate that even spin-forbidden and invisible (dark) states in non-resonant PES can be observed by PES at the resonances with strong singlet-triplet mixing via spin-orbit coupling of the 2p core electrons.

All experiments were carried out at varied-line-spacing plane grating monochromater beamline BL4B. Photoabsorption spectra are taken by measuring transmitted photon intensity using Si diode. A few Torr CS_2 gas pressure was separated by 1200 Å polyimide filter. Photon energy is calibrated by measuring Ar $2p_{3/2}$-4s* and Kr $3d_{3/2}$-5pabsorption peaks at 244.4 and 92.425 eV, respectively. Angle-resolved photoion yield spectra (ARPIS) were measured by two channeltrons set in the 0° (parallel) and 90° (perpendicular) directions relative to the electric vector of the linearly polarized light. Retardation grids were used to detect energetic photoions (>3 eV). PES spectra were measured by a SES-200 analyzer, where the observed electron momentum is parallel to the electric vector of the linearly polarized light.

Figure 1 shows high-resolution photoabsorption and ARPIS spectra of CS_2. Distinct anisotropy is observed above 165 eV, in sharp contrast to the lower S $2p\rightarrow3\pi_u$* resonances. These information on symmetry of excited states combined with *ab initio* theoretical investigation provides detail insight on the competition of spin-orbit and exchange interactions. Here, we focus on PES and do not discuss on ARPIS results further. Similar discussion is presented in this issue for SO_2.

Figure 2 shows PES recorded at S $2p_{3/2}\rightarrow3\pi_u$* resonance and non-resonant PES below the resonance. The ground state CS_2 has $\cdots(6\sigma_g)^2(5\sigma_u)^2(2\pi_u)^4(2\pi_g)^4$ electronic configuration in $D_{\infty h}$. Main bands, $^2\Pi_g$, $^2\Pi_u$, $^2\Sigma_u$, $^2\Sigma_g$ states are observed. Satellite bands 0, 1", 2, 2', 2", 3, and higher-energy structures are clearly enhanced, whereas satellites 1, and 1' are not. Here satellite numbering 1, 1', 2 and 3 follows the previous study[1]. In the high-resolution spectra (Figure 3), these satellites 1-3 are clearly resolved. Satellites 0, 1", 2', and 2" have not been found in the previous studies measured at excitation energies below 100 eV.

Within the (*LS*) coupling scheme, excited state of S $2p_{3/2}\rightarrow3\pi_u$* transition is described as strongly mixed state with singlet and triplet non-relativistic states, where the intensity comes from dipole-allowed singlet non-relativistic state. Intermediate states in the resonant PES have a large triplet contribution, which opens up transitions to ionized quartet states in addition to doublet states. Satellite 0 is not observed in non-resonant spectrum; therefore it can be assigned to the transition to a quartet state. Satellite 1 is assigned to the lowest doublet shake-up state with $^2\Pi_u$ symmetry [1,2] allowed in the non-resonant PES spectra. Satellite 0 is possibly explained as transition to the quartet ionized states $^4\Pi_u$ with a dominant $\cdots(6\sigma_g)^2(5\sigma_u)^2(2\pi_u)^4(2\pi_g)^2(3\pi_u)^1$ configuration. Difference in spin state makes the quartet satellite 0 lower than its counterpart doublet satellite 1.

In summary, we have measured ARPIS and resonant PES of CS_2. We have successfully found quartet shake-up state in the resonant PES via the S $2p_{3/2}\rightarrow3\pi_u$* resonance. The spin-orbit mixing in the intermediate state opens up transitions to dark states such as quartet shake-up.

References

[1] P. Baltzer, B. Wannberg, M. Lundqvist, L. Karlsson, D.M.P. Holland, M.A. MacDonald, M.A. Hayes, P. Tomasello, W. von Niessen, Chem. Phys. 202 (1996) 185.

[2] J. Schirmer, W. Domcke, L.S. Cederbaum, W. von Niessen, L. Åsbrink, Chem. Phys. Lett., 61 (1979) 30.

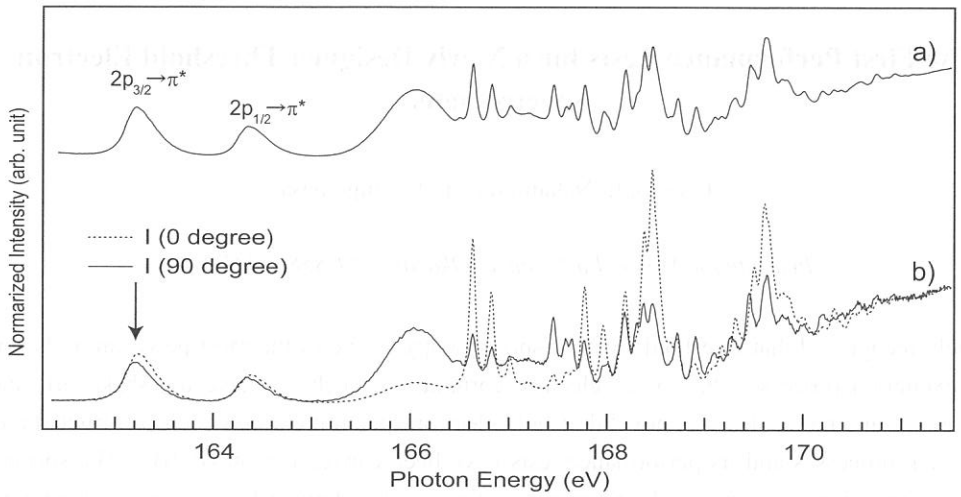

Figure 1. Photoabsorption Spectrum (a) and angle-resolved ion yield spectra (b) of CS_2. Resonant photoelectron spectra are measured at the excitation energy indicated as an arrow.

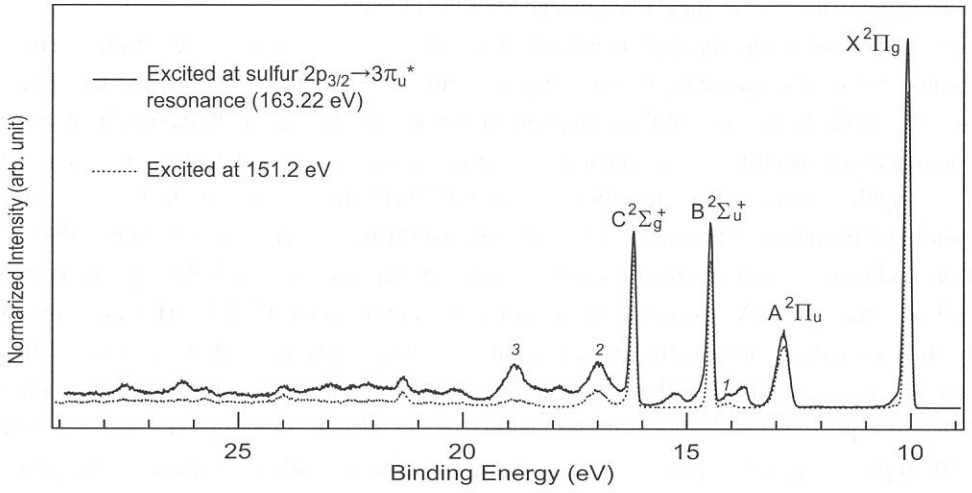

Figure 2. Low-resolution resonant photoelectron spectrum of CS_2 recorded at $2p_{3/2}\rightarrow3\pi_u*$ resonance (163.22 eV). Non-resonant photoelectron spectrum recorded below sulfur 2p excitation region (151.2 eV) is shown for comparison.

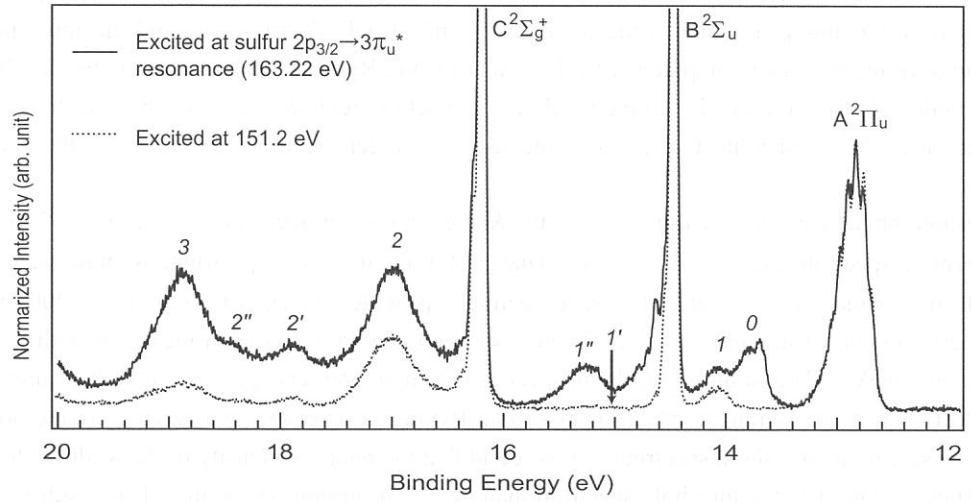

Figure 3. High-resolution resonant photoelectron spectrum of CS_2 recorded at $2p_{3/2}\rightarrow3\pi_u*$ resonance (163.22 eV). Non-resonant photoelectron spectrum recorded below sulfur 2p excitation region (151.2 eV) is shown for comparison.

(BL4B)

The First Performance Tests for a Newly Designed Threshold Electron Spectrometer

T. Gejo, E. Nakamura, and E. Shigemasa

Institute for Molecular Science, Okazaki 444-8585, JAPAN

It is widely recognized that threshold electron spectroscopy is one of the most powerful tools for probing the multiple excitation processes due to the electron correlations, such as shake up, shake off, and double ionization, in atoms and molecules. A novel threshold electron spectrometer has been constructed recently for investigating such processes and its performance tests have been carried out on BL4B. The spectrometer is composed of an input lens system based on the penetrating field technique [1] and an electrostatic analyzer (Comstock inc. AC-901 model). The lens system was designed for optimum collection and focusing of low energy electrons. By performing suitable adjustment of the potentials applied to the grids of the lens, it is possible to collect and focus electrons with energies from 0 to about 10 eV. Electrons passing through the analyzer were detected by a micro channel plate placed after the exit slit.

The spectra obtained in the present measurements correspond to constant electron energy spectra. Namely, the photon energy was ramped across the region of interest, while the collection energy of the analyzer was held fixed. When the fixed value of the collection energy was made equal to 0, the resultant spectrum was a threshold photoelectron spectrum. To enhance the performance for detecting threshold photoelectrons a draw-out field was applied between the interaction region and the entrance to the lens stack [1]. Unfortunately the actual threshold performance of the analyzer has not been confirmed so far, since it is impossible to measure the threshold photoelectron spectrum of rare gases in their first ionization threshold regions, whose natural widths are much less than 10 meV, using the monochromatized radiation at BL4B. However, by comparing the previously measured threshold electron spectrum in Kr 3d near-threshold photoionization [2] with that measured by our analyzer, estimation of the energy resolution of the analyzer becomes possible. Fig. 1 shows the threshold electron spectrum of Kr atoms in the vicinity of the 3d ionization region, measured with the slit openings of 120-50 μm. The corresponding photon energy resolution is about 50 meV. The peak width of the 5p Rydberg state in Fig. 1 is about 135 meV which is due to the natural width of the state (~100 meV) and the finite energy width of the incident radiation and the analyzer. Assuming that the total width observed can be expressed as the vector sum of the individual contributions with Gaussian profiles, it seems safe to say that the energy resolution of the analyzer is better than 80 meV. It is obvious from the spectrum of Fig. 1 that the threshold spectrum contains peaks due to the ionic states and also Rydberg states, and the ionic peaks are broadened and asymmetric when compared with the peaks for the Rydberg states. This is the result of post collision interaction (PCI), which is due to the Coulomb interaction between the slow photoelectron produced by the primary near-threshold ionization process and the fast Auger electrons generated by the subsequent decay process.

The threshold photoelectron spectrum of N_2 in the *K*-shell excitation region is shown in Fig. 2 along with the photoabsorption spectrum except for the π^* resonance. For the threshold spectrum, asymmetric slit widths of 125 and 50 μm for the entrance and exit slits, respectively, provide an energy resolution of ~200 meV over the photon energy region of interest, while the photoabsorption spectrum has been measured with the energy resolution of ~60 meV. The similar threshold spectrum with poorer energy resolution has already been reported in Ref. 3. The prominent π^* resonance and Rydberg transitions converging to the ionization threshold are present in the threshold spectrum. It is found that the relative intensity of the Rydberg transitions to higher n states are larger in the threshold spectrum than in the absorption spectrum. This result is common to the atomic case, where relative probability for an excited state for undergoing shake off increases with greater n. The peak corresponding to the N 1s threshold photoelectrons exhibits the energy shift to higher energy side

and asymmetry due to the PCI effect. There are at least two additional broad bands centered at ~415 and ~420 eV in the threshold spectrum, where the double excitations and σ* shape resonance are observed in the absorption spectrum. For further detailed discussions on these structures, improvement on the total performance of the experimental setup and additional information on the excited states are obviously necessary.

References

[1] R.I. Hall et al., *Meas. Sci. Tech.* **3**, 316 (1992).

[2] L. Avaldi et al., J. *Phys. B* **24**, 427 (1991).

[3] L.J. Medhurst et al., *J. Chem. Phys.* **89**, 6096 (1988).

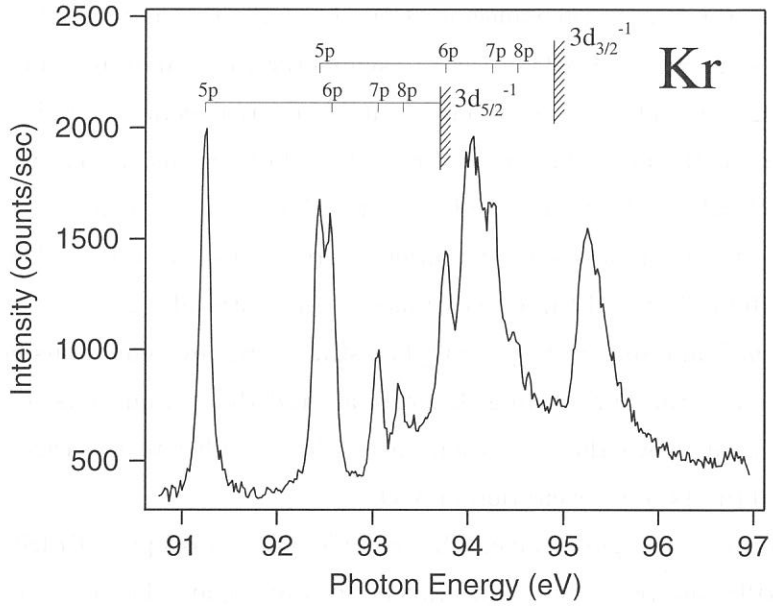

Fig. 1. Threshold photoelectron spectrum obtained in the region of the 3d subshell of Kr.

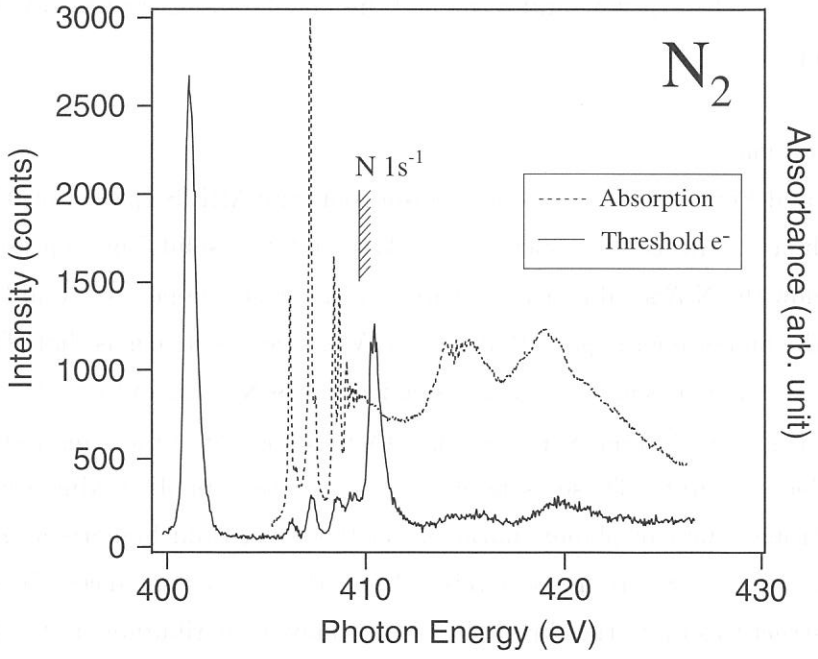

Fig. 2. Threshold photoelectron spectrum obtained in the *K*-shell excitation region of N_2.

(BL4B)

Angle-resolved photoion spectra of NO_2 in the N *K*-edge region

T. Gejo, E. Shigemasa, M. Nagasono, H. Oji, T. Hatsui and N. Kosugi

Institute for Molecular Science, Myodaiji, Okazaki 444-8585, Japan

Introduction

The NO_2 molecule has a bent structure with terminal oxygen atoms and belongs to the point group C_{2v}. Comparing to other liner tri-atomic molecules, NO_2 has one additional electron as an unpaired electron to the linear molecules CO_2 of the $D_{\infty h}$ symmetry with three unoccupied orbitals, $2\pi_u^*$, $5\sigma_g^*$, and $4\sigma_u^*$, and N_2O of the $C_{\infty v}$ symmetry with three unoccupied orbitals, $3\pi^*$, $8\sigma^*$, and $9\sigma^*$. The $(2\pi_u^*)^1$ and $(3\pi^*)^1$ states of CO_2 and N_2O are degenerate and are stabilized in a bent geometry due to the Renner-Teller effect, where $2\pi_u^*$ of CO_2 is split into in-plane π^* ($6a_1^*$) and out-of-plane π^* ($2b_1^*$), where the former and the latter have bent and linear stable geometries, respectively, and the former is lower in excitation energy than the latter. Thus, NO_2 has one half-filled valence orbital $6a_1^*$ and three unoccupied valence orbitals, $2b_1^*$, $7a_1^*$, and $5b_2^*$, which correspond to $3b_1^*$, $9a_1^*$, and $6b_2^*$ in SO_2. NO_2 has still strong covalent bonds between N and O even with an electron in the antibonding $6a_1^*$ orbital, and the N and O 1s$\rightarrow 5b_2^*$ excitation is expected to be observed above the ionization thresholds, similar to the case of the 1s$\rightarrow 4\sigma_u^*$ excitation in CO_2 and the 1s$\rightarrow 9\sigma^*$ excitation in N_2O.

Here we report the angle-resolved photoion yield spectroscopy (ARPIS) of NO_2 in the N *K*-edge region. ARPIS spectroscopy is a useful tool to investigate the symmetry of the K-shell excited states. In electric dipole transitions induced by the linearly polarized light, the transition probabilities relate to the molecular orientation with respect to the direction of the electric vector of the incident light . The experimental setup and the calculation procedure have been described in the previous report.

Results and Discussion

Fig. 1a and Fig. 1b display the photoabsorption and ARPIS spectra of NO_2 in the N *K*-edge region with a resolution of ~3000. The dots and the solid line represent I_{90} and I_0, respectively. Below the N *K*-shell ionization thresholds, two strong peaks, A and B, are observed. The intensity of the higher-energy peak B at 403.26 eV is twice as strong as that of the lower peak A at 401.03 eV. The higher peak B is easily assigned to the N 1s $2a_1\rightarrow 2b_1\pi^*$ (B_1) transition, and the lower peak A is assigned to the N 1s $2a_1\rightarrow 6a_1^*$ (A_1), as a result of the unpaired electron in the half-filled $6a_1$ valence orbital. These assignments are also reasonable, taking account of weak Σ (in plane) and strong Π (out of plane) characters of the lower- and higher-energy peaks in the ARPIS spectra as shown in Fig.1b, respectively. Above these two resonances, the spectra exhibit relatively weak structures up to the thresholds, which may be attributable to the Rydberg states and the Rydberg-valence mixed states. The excitation to $7a_1^*$ is expected to be less contributive to the spectral intensity, considering that $7a_1^*$ of NO_2 corresponds to $5\sigma_g^*$ in CO_2 and $8\sigma^*$ in N_2O

with s-type character on the central atom and the excitation from the K-shell to the s-type state should be weak. In the continuum, only one broad band around 416 eV is observed and is attributed to a σ^* continuum shape resonance originating from the strong σ* anti-bonding orbital of $5b_2$*.

Fig. 1c represents the blowup of the photoabsorption spectra of NO_2 in the N K-edge region with a resolution of ~5000. The calculations indicate that the valence and Rydberg transitions converging to the triplet ionization threshold are dominant. The triplet and singlet separation is observed for the 3s Rydberg states, C and D, where the total spin coupling is doublet and the exchange effect involving the Rydberg electron is estimated to be 0.18 eV at the most from the difference in their term values. Furthermore, the calculations show that the $7a_1$* valence is completely dissolved in the Rydberg sea and cannot be assigned to a specific peak. The $7a_1$* valence is mainly mixed into the s-type Rydberg, especially the 3s and 4s Rydberg (assigned to features C and G in Fig. 1), but the intensity contribution is expected to be small, as mentioned above. The features E/F, I/J, and M are mainly attributed to p-type Rydberg transitions converging to the triplet ionization threshold. Moreover, it is found from the calculations that the 1s→d$b_1(\pi)$ triplet channel is relatively strong among the 1s→d-type transitions and the features H, L and P have the same type of contributions.

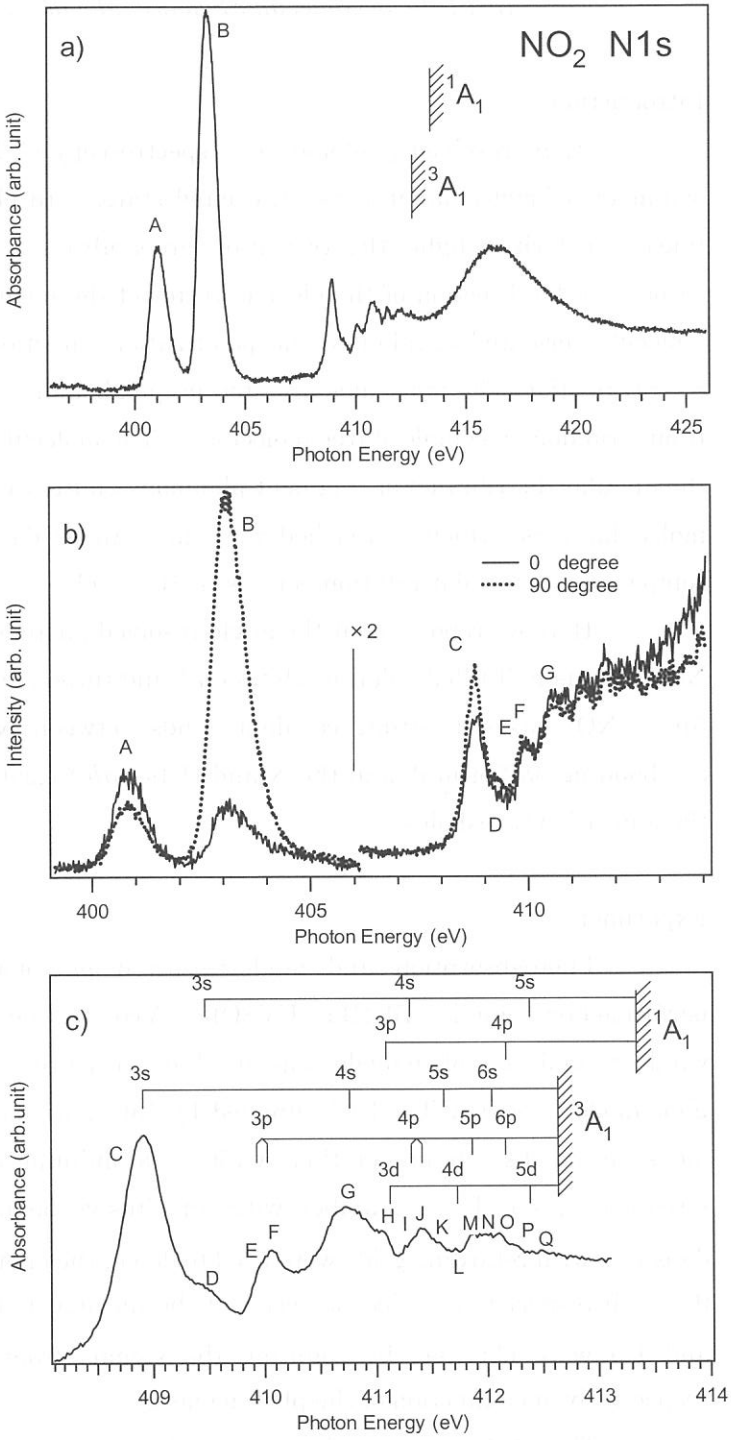

Figure 1. a) Absorption spectrum of NO_2 in the N K-edge region. b) Angle-resolved ion yield spectra of NO_2. Dotted and solid lines denote I_{90} and I_0 ion yields, respectively, in the N K-edge region. c) Absorption spectrum of NO_2 in the Rydberg excitation region.

(BL4B)

Angle-resolved photoion spectra of NO_2 in the O *K*-edge region

T. Gejo, E. Shigemasa, M. Nagasono, H. Oji, T. Hatsui and N. Kosugi

Institute for Molecular Science, Myodaiji, Okazaki 444-8585, Japan

Introduction

Angle-resolved photoion yield spectroscopy (ARPIS) is a useful tool to investigate the symmetry of molecular inner-shell excited states. In electric dipole transitions induced by the linearly polarized light, the transition probabilities relate to the molecular orientation with respect to the direction of the electric vector of the incident light. For the $\sigma\rightarrow\sigma$ transitions the molecules oriented parallel to the polarization direction are selectively excited, while for the $\sigma\rightarrow\pi$ transitions the molecules oriented perpendicular to the direction are preferentially excited from a random ensemble of free molecules. The molecular orientation will be directly reflected in the angular distribution of fragment photoions emitted immediately from a repulsive potential of molecular ions, which is reached by a fast Auger decay of the *K*-shell vacancy ($\tau\sim10^{-14}$ sec) compared to molecular rotation periods ($\tau\sim10^{-10}$ sec).

Here we report about the angle-resolved photoion spectra of NO_2 in the O *K*-edge region. NO_2 has one half-filled valence orbital $6a_1$* and three unoccupied valence orbitals, $2b_1$*, $7a_1$*, and $5b_2$*. NO_2 has still strong covalent bonds between N and O even with an electron in the antibonding $6a_1$* orbital, and the N and O 1s$\rightarrow5b_2$* excitation are expected to be observed above the ionization thresholds.

Experiment

Photoabsorption and angler-resolved photoion yield (ARPIS) measurements were performed on beamline BL4B at UVSOR. A conventional gas cell system having leak tight thin windows and the photodiode was used to measure the photoabsorption spectra. A silicon photodiode (model AXUV-100) supplied by International Radiation Detectors Inc. was used to measure the absolute photon flux. A 1500 Å aluminum window from Luxel is installed to the up stream of gas cell. A chamber with an effusive beam nozzle was used. Two identical ion detectors with retarding grids were used to detect the energetic photoions (>2eV) emitted at 0° and 90° with respect to the electric vector of the incident light, respectively. The ARPIS spectra (I_0 and I_{90}) were obtained by counting the signals from the 0° and 90° positioned detectors, respectively, as a function of the photon energy.

The O 1s core-to-valence excited states of NO_2 were calculated by multi-reference configuration interaction including single and double excitations (MR-SDCI) [1]. The molecular geometries for the calculations were taken from those for the ground states. The CI calculations were carried out using SCF (self consistent field) orbitals for the 1s ionized states, which were obtained from the use of the GSCF3 code [2,3]. Symmetry-adapted molecular orbitals were used

even for the O 1s excited states with a localized character, which can be taken into account through MR-SDCI.

Results and discussion

Fig. 1a shows the photoabsorption spectrum of NO_2 in the O *K*-edge region with an energy resolution of ~5000. Fig. 1b demonstrates the ARPIS spectra with a resolution of ~3000. The dots and the solid line denote I_{90} and I_0, respectively. The splitting caused by the interaction between two O 1s orbitals ($1b_2$ and $1a_1$) is expected to be negligible. The lowest two features A and B are simply assigned to the O 1s $1a_1/1b_2 \rightarrow 6a_1^*(A_1,B_2)$ and O 1s $1a_1 \rightarrow 2b_1^*(B_1)$ transitions, respectively, where the O 1s $1b_2 \rightarrow 2b_1^*(A_2)$ transition is dipole forbidden. Fig. 1a shows rather strong features in the Rydberg excitation region, and a comparatively strong and broad enhancement above the ionization thresholds. The latter is assigned to the O 1s$\rightarrow 5b_2^*$ shape resonence, though Jürgensen and Cavell [4] assigned the shape resonance to the a_1 symmetry.

The excited states converging to the triplet ionized state are lower in energy than the states converging to the singlet. Similar to the case of the N 1s excitation, the calculations manifest that the $7a_1^*$ valence is completely dissolved in the Rydberg sea and cannot be assigned to a specific peak. The $7a_1^*$ valence is mainly mixed into the s-type Rydberg, especially the 4s and 5s Rydberg (assigned to the features D and E in Figure 1). In contrast to the central N 1s excitation, the terminal O 1s to $7a_1^*$ excitation is strongly contributive to the spectral intensity, as discussed in the O 1s and terminal N 1s excitations of CO_2 and N_2O.

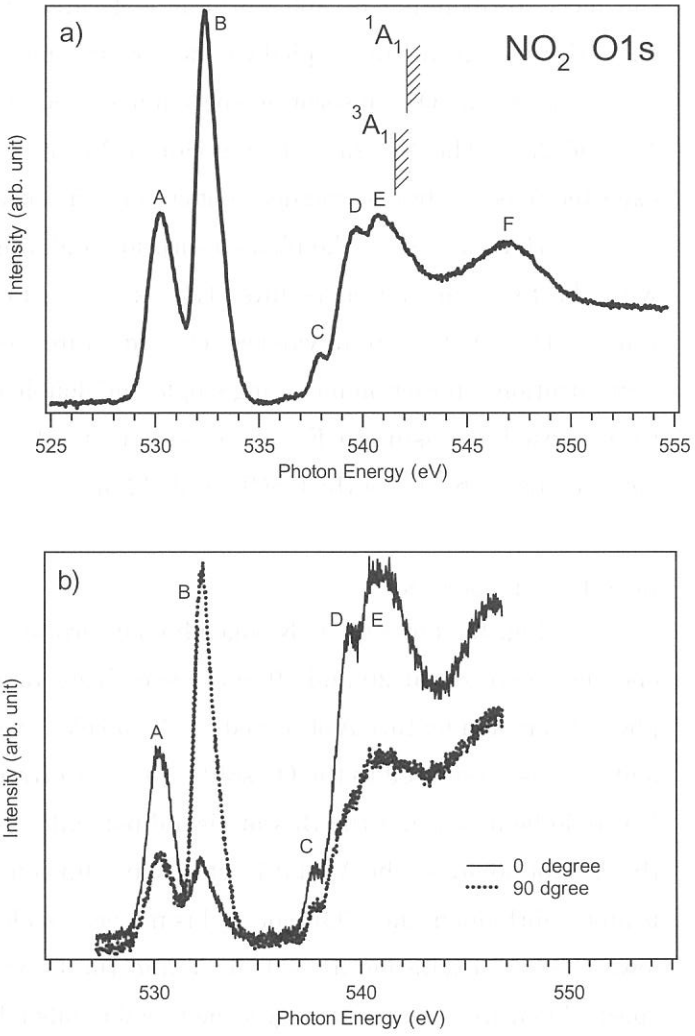

Figure 1. a) Absorption spectrum of NO_2 in O *K*-edge region. b) Angle-resolved ion yield spectra of NO_2 in the O *K*-edge region. Dotted and solid lines denote I_{90} and I_0 ion yields, respectively.

References

[1] E. Rühl et al., *J. Chem. Phys.* 116 (2002) 3316. [2] N. Kosugi and H. Kuroda, *Chem. Phys. Letters.*, 74 (1980) 490. [3] N. Kosugi, *Theoret. Chim. Acta*, 72, (1987) 149. [4] A. Jürgensen and R.G. Cavell, *Chem. Phys.* 257 (2000) 123.

(BL4B)

Angle-resolved photoion spectra of SO_2

T. Gejo, E. Shigemasa, M. Nagasono, H. Oji, T. Hatsui and N. Kosugi
Institute for Molecular Science, Myodaiji, Okazaki 444-8585, Japan

Introduction

The SO_2 molecule has three unoccupied valence orbitals, $3b_1$*, $9a_1$* and $6b_2$*, which can be associated with the three S 3p orbitals, where SO_2 has an electronic structure of $S^{4+}[(3s)^2(3p)^0]\cdot(O^{2-})_2$ in the limit of an ionic bonding picture and the $3b_1$, $9a_1$ and $6b_2$ orbitals correspond to out-of-plane S3p π (π_{out}), in-plane S3p π (π_{in}) and in-plane S3p σ, respectively [1]. All the S1s ($1a_1$) excitations to the $3b_1$*, $9a_1$* and $6b_2$* orbitals are dipole-allowed and are found to be lying below the S1s→Rydberg excitations with the term values of 10.4, 5.7, and 4.8 eV, respectively [1]. The chemical bond between S and O is not so strong, and even the excitation to the most antibonding σ* ($6b_2$) orbital is located below the ionization threshold. The single excitations to all the unoccupied valence orbitals are observed below the ionization threshold even in the case of the O1s absorption spectra assigned previously, though there are two O 1s orbitals, $1b_2$ and $2a_1$. The $1b_2$–$2a_1$ splitting caused by the interaction between the two O 1s orbitals is expected to be negligible and does not change the situation.

Here we report the photoabsorption and anlgle resolved photoion specta of SO_2, together with the SCF calculation results. The experimental setup has been described at the previous report. The O 1s core-to-valence excited states of SO_2 were calculated by multi-reference configuration interaction including single and double excitations (MR-SDCI). The CI calculations were carried out using SCF (self consistent field) orbitals for the 1s ionized states, which were obtained from the use of the GSCF3 code [2,3].

Results and discussion

Fig. 1a shows the O K-edge photoabsorption spectrum of SO_2. The entrance and exit slit openings were set at 20 and 10 μm, respectively, to get a resolving power of ~5000. The lowest photoabsorption feature A observed at 530.56 eV is well separated from the higher features. The feature A is attributed to the O 1s$\sigma(2a_1)$→$\pi^*(3b_1)$ transition, considering its term value of 9.27 eV. It should be noted that the B_1 state is a dipole-allowed out-of-molecular plane (π*) transition from the A_1 ground state, the A_1 and B_2 states are dipole-allowed in-plane transitions, and the A_2 state is dipole-forbidden; the $\pi^*(3b_1)$ orbital is not accessible from the O 1sσ ($1b_2$) electron. Between the lowest 1s→π* excitation at 530.56 eV and the O K-shell ionization threshold at 539.83 eV, the spectral feature is dominated by some broad bands labeled as B, C, and D at ~535 eV (term values of ~5eV) arising from the 1s→in-plane excitations, which consist of the O 1s→$9a_1$* (dipole-allowed B_2 from $1b_2$ and A_1 from $2a_1$) and O 1s→$6b_2$* (dipole-allowed A_1 from $1b_2$ and B_2 from $2a_1$) transitions. The structures E, F, and G are comparatively weak and have term values of 2.24, 1.63, and 0.75 eV, respectively; therefore, they are possibly assigned to the lowest s-type (4s or 5s)

and p-type (4p or 5p) Rydberg transitions. In the continuum, two broad bands are observed around 540.80 and 542.69 eV, which are attributable to double excitations or S 3d-type shape resonances, because there are no other singly excited valence states than the $1s \rightarrow 3b_1^*$, $9a_1^*$ and $6b_2^*$ transitions.

Fig. 1b indicates the present O K-edge ARPIS spectra of SO_2, where the dots and the solid line represent I_{90} and I_0, respectively. The peak A is definitely assigned to the O $1s(2a_1) \rightarrow \pi^*(3b_1)$ excitation, and F is assigned to the O $1s(2a_1) \rightarrow 4pb_1$ or $5sa_1$ Rydberg excitation ($B_1 \leftarrow A_1$). The peak G is probably assigned to the O $1s(1b_2/2a_1) \rightarrow 4pa_1$ and $4pb_2$ Rydberg excitations. However, the features B, C and D in Fig. 1 are difficult to assign even with the help of the ARPIS spectra.

In order to assign these peaks more accurately we have performed the SCF-CI calculations. The calculated results show that both the $1b_2 \rightarrow 9a_1^*$ (B_2) and $2a_1 \rightarrow 9a_1^*$ (A_1) transitions contribute to the feature B but $1b_2 \rightarrow 9a_1^*$ (B_2) is much stronger than $2a_1 \rightarrow 9a_1^*$, and that both the $1b_2 \rightarrow 6b_2^*(A_1)$ and $2a_1 \rightarrow 6b_2^*(B_2)$ transitions contribute to the feature C but $1b_2 \rightarrow 6b_2^*(A_1)$ is much stronger. That is, the $9a_1^*$ orbital is lower in energy than the $6b_2^*$ orbital, similarly to the case of the S 1s excitation [1]; however, the excitations from the b_2-symmetry core orbital are dominant in the case of the O 1s excitation, resulting in the inverse retarding potential dependence of the asymmetry prameters for $9a_1^*$ and $6b_2^*$ in comparison with the S 1s (a_1) excitation. The feature D is assigned to the O $1s(1b_2/2a_1) \rightarrow 4sa_1$ Rydberg excitation. The calculation also shows that E is assigned to the O $1s(2a_1) \rightarrow 4pb_1$ or O $1s(1b_2/2a_1) \rightarrow 4pa_1$ Rydberg excitation and F is assigned to the O $1s(1b_2/2a_1) \rightarrow 4pb_2$ or O $1s(2a_1) \rightarrow 3db_1$ Rydberg excitation.

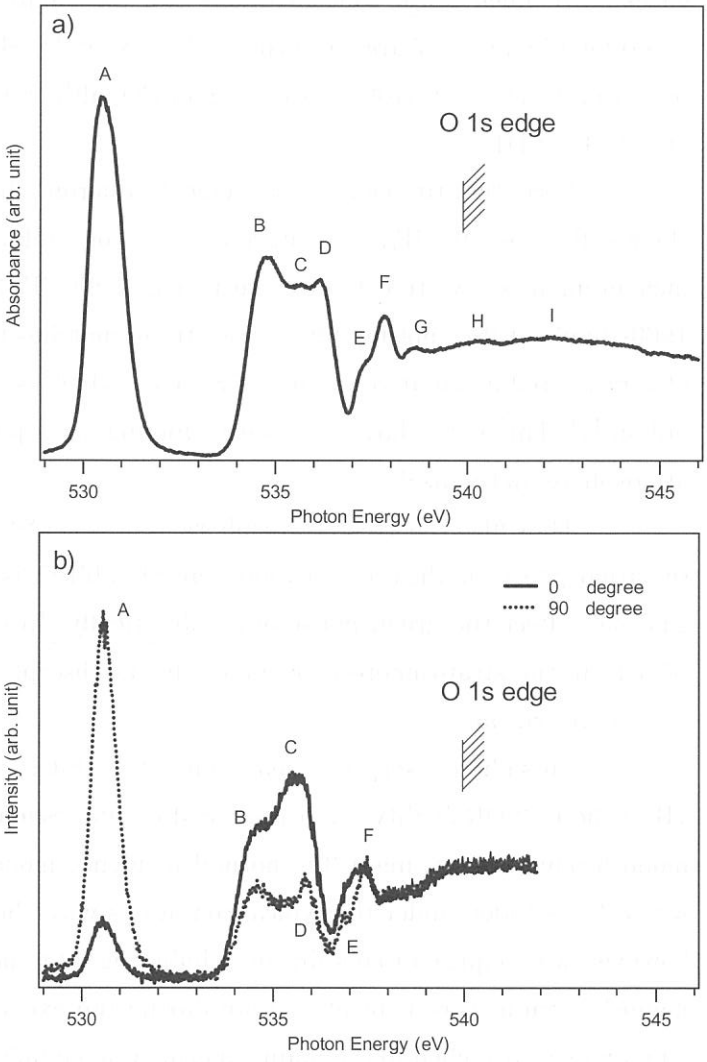

Figure 1. a) Absorption spectrum of SO_2 in the O K-edge region. b) Angle-resolved ion yield spectra of SO_2. Dotted and solid lines denote I_{90} and I_0 ion yields, respectively.

References

[1] J. Adachi et al. Chem. Phys. Letters, 294 (1998) 559. [2] N. Kosugi and H. Kuroda, Chem. Phys. Letters., 74 (1980) 490. [3] N. Kosugi, Theoret. Chim. Acta, 72, (1987) 149.

(BL7B)

The measurement of absorption spectra of Trifluoromethyl Sulfur Pentafluoride in VUV region

Tatsuo GEJO, Eiji SHIGEMASA , Kenshi TAKAHASHI [A)] and Yutaka MATSUMI [A)]
Institute for Molecular Science, Myodaiji, Okazaki 444-8585, Japan
[A)]STEL, Nagoya Univ. Honohara 3-13, Toyokawa, 442-8507, Japan

Global warming or green house effect is one of the major issues for environmental chemistry. Although CO_2, CH_4, and N_2O play a major role on the green house effect in air, some gases with much lower concentrations can contribute to the global warming because of their exceptionally large infrared absorption. For example, SF_6 has 22,200 times larger global warming potential (GWP) over a100-year time than CO_2 although it is currently present in the atmosphere at only 4 ppt [1].

Recently Sturges et al. detected Trifluoromethyl sulfur pentafluoride (SF_5CF_3), which is chemically close to SF_6, at Antarctic deep consolidated snow (firn) [1]. This Antarctic firn measurement shows that the concentration of SF_5CF_3 have increased from near zero in the late 1960s to about 0.12 ppt in 1999, whose trend matches to recent global warming tendency. They also measured a radiative forcing of SF_5CF_3, which is 0.57 watt per square meter per parts per billion [1]. This is the largest radiative forcing, on a per molecule basis, of any gas found in the atmosphere up to this date.

They also reported stratospheric profiles of SF_5CF_3 and suggested that it is long-lived in the atmosphere (on the order of 1000 years) [1]. If this is true, the irreversible accumulation of this gas may affect the green house effect drastically. In order to access this effect and lifetime of SF_5CF_3 in the stratosphere more precisely, its absorption spectra and cross sections in the VUV region are crucial.

This photoabsorption measurement of SF_5CF_3 in VUV region was performed at Beamline 7B in the UVSOR facility, Institute for Molecular Science. Synchrotron radiation at UVSOR was monochromated by using a 3-m normal incidence monochromator (NIM). The energy resolution was $\lambda/\Delta\lambda$ = 10000 under the typical conditions with the slit widths of 100 μm. High photon flux, however, was required to obtain the reliable signal to noise ratio and hence the slit widths of the monochromator were kept at 500 μm during the experiment. A photoabsorption cell was 33 cm long and was attached to the main experimental chamber. The typical sample pressure in the cell was 10 Pa, which was measured by a Baratron manometer. An LiF filter with a thickness of 1.5 mm was installed in front of the cell in order to keep the monochromator in good vacuum condition. The intensity of the photon beam transmitted through the cell was monitored by using a silicon photodiode (IRD Inc, AXUV-100). The photoabsorption cross sections were calculated by using the Beer-Lambert expression. The data were checked to ensure there is no line saturation effect.

Fig 1 shows the absorption spectra of SF_5CF_3 in VUV region. In this figure, two strong peaks were observed: One peak around 107 nm (A) and another one around 130 nm (B). The peak similar to A is also observed in SF_6, whereas the equivalent to the peak B was not observed. Therefore one can suggest that the peak B arises from the transition from the lone pair electron of CF_3.

Based on these data, we will estimate the lifetime of SF_5CF_3 in the stratosphere.

[1] W. T. Sturges et al., Science 289, 613(2000)

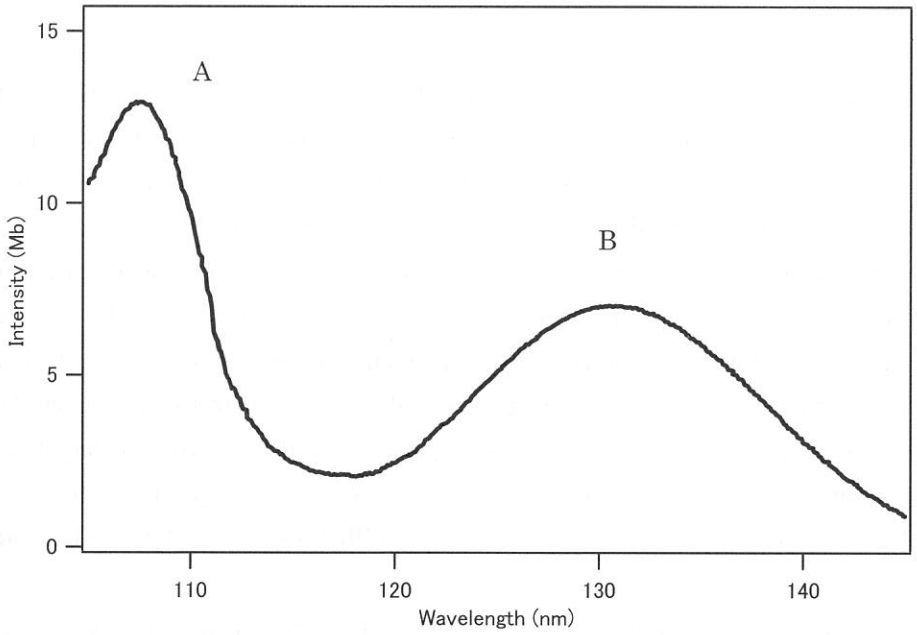

Fig. 1: The absorption spectra of SF_5CF_3 in the VUV region

(BL8B1)

Molecular size effect on the site-specific fragmentation of the N and O *K*-shell excited oxoalkanenitrile molecules

Tomoki MORITA, Kazumasa OKADA, Toshio IBUKI,[a] Yuichi HAGA,[a] Shuichiro TANIMOTO, Tatsuo GEJO,[b] Ko SAITO, and Keiichi OHNO

Department of Chemistry, Hiroshima University, Higashi-Hiroshima 739-8526

[a] *Kyoto University of Education, Kyoto 612-8522*

[b] *Institute for Molecular Science, Okazaki 444-8585*

An attractive concept of photochemistry is selective bond activation of a molecule by tuning the photon energy to specific electronic and/or vibrational transitions. Monochromatized soft x-ray synchrotron radiation can excite core electrons of a molecule. Because of the localized nature of core electrons, an intriguing possibility is that the bond rupture will be also localized around the atomic site of excitation. Evidence for such selective photochemistry has been found in studies on the fragmentation of a few molecules since the pioneering work by Eberhardt et al. [1], showing the C^+ and O^+ fragment ions were characteristically enhanced in the carbonyl C(1s) $\rightarrow \pi^*$ excited acetone. The question then arose as to the correlation of the created core hole and the removal of valence electrons via Auger decay with the molecular fragmentations. In later studies, it became apparent that the selectivity is largely determined by the electronic decay of the core-hole state [2]. Since then, relatively large number of studies has been performed with an Auger electron–photoion coincidence (AEPICO) technique for detailed understanding of the fragmentation mechanisms.

On the other hand, the idea of chemical activation and the non-statistical effects on reaction emerged up in the field of unimolecular reactions [3]. Dissociation pattern can be viewed as the outcome of the competition between the bond rupture in the activated site and energy randomization over the activated molecule. Thus in order to have more insights into the site-specific photochemistry of core-excited molecules, it is of great interest to determine whether the initial memory of core excitation preserves against the energy randomization. In our recent study on the fragmentation of the N and O *K*-shell excited CH_3OCOCN and CH_3OCOCH_2CN molecules, the fragmentation patterns were essentially identical for the smaller molecule, while marked site-specific fragmentation was observed for the other molecule [4]. This result infers that the site-specific fragmentation following core excitation depends on the molecular size. In this report, we present the results of a consecutive study concerning the molecular size effect on the site-specific fragmentation following the excitation of core electrons in a polyatomic molecule.

The experiments were performed on the beamline BL8B1 at the UVSOR facility. Photoabsorption spectra were observed in the N and O *K*-shell regions of gaseous pyruvonitrile (CH_3COCN), cyanoacetone (CH_3COCH_2CN), and 4-oxopentanenitrile ($CH_3CO(CH_2)_2CN$) molecules. A Samson-type ion chamber with 10-cm long electrodes was mounted on the main chamber and used for the measurement. The ion current was fed to a picoammeter and stored in a personal computer, together with the sample pressure. The energy scale was calibrated using the major soft x-ray peaks of N_2 and O_2.

The photoelectron–photoion coincidence (PEPICO) spectra were acquired at some typical photon energies by using a reflectron type time-of-flight (RTOF) mass spectrometer. An effusive flow of sample

gas was introduced into the main chamber through a gas nozzle orthogonal to both the photon beam axis and the spectrometer tube. A high electrostatic field was applied across the collision region so as to collect the energetic fragment ions with kinetic energies up to ≅10 eV. The flight time of ions was measured with a TAC. The output pulse height from the TAC was analyzed with an MCA and the obtained spectrum was then transmitted to a personal computer. The axis of the spectrometer was set at the magic angle with respect to the photon polarization direction for suppressing anisotropic effect in the photoabsorption process. An Al thin filter was inserted upstream in order to reduce the scattered stray light. Incident soft x-ray flux was monitored by an Au mesh and recorded simultaneously as the photocurrent. All spectra were normalized by the photocurrent in order to correct for fluctuations in dispersed photon flux. The CH_3COCN sample for the experiment was obtained commercially and the other two samples were prepared according to the published methods [5, 6].† All samples were used after being degassed by several freeze–pump–thaw cycles.

Figure 1 shows the RTOF mass spectra acquired at the $N(1s)^{-1}$ and $O(1s)^{-1}$ ionizations of gaseous $CH_3CO(CH_2)_2CN$ molecule. The photofragment ions heavier than m/e=60 were negligible. Clear dependence of the photofragmentations on the atomic site of excitation can be found in the present study as well. It is worthwhile to note that the abundant photofragment ions are H^+ and CN^+ at the N *K*-shell ionization, while heavier photofragments such as the CH_3C^+ and CH_3CO^+ ions are greatly produced at the O *K* edge: The yields of the latter two photofragments are 1.5 and 2.4 times larger in the $O(1s)^{-1}$ ionization than those in the $N(1s)^{-1}$ ionization, respectively. The abundant production of these photofragment ions is reasonably explained by the bond fission around the carbonyl group. That is, for the $CH_3CO(CH_2)_2CN$ molecule the photofragmentation basically occurs at the limited site of initial excitation. By contrast, core excitation of the smallest CH_3COCN molecule does not show any difference in fragmentation patterns regardless of the sites and states of the initial excitation. Core-excited CH_3COCH_2CN molecule gives the middle result among the molecules studied.

†The authors are grateful to Mr. M. Yamashita and Professor Y. Yamamoto at Hiroshima University for their help in the synthesis of the samples.

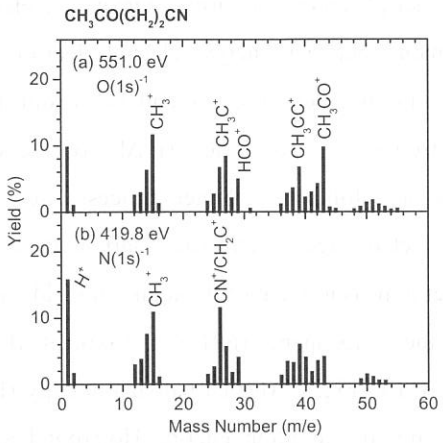

Fig. 1: The RTOF mass spectra of $CH_3CO(CH_2)_2CN$ excited at the $O(1s)^{-1}$ and $N(1s)^{-1}$ ionizations. The spectra are presented as percentage yields calculated from the peak areas.

References

[1] W. Eberhardt, T. K. Sham, R. Carr, S. Krummacher, M. Strongin, S. L. Weng, and D. Wesner, *Phys. Rev. Lett.* **50**, 1038 (1983).

[2] W. Eberhardt, E. W. Plummer, I.-W. Lyo, R. Reininger, R. Carr, W. K. Ford, and D. Sondericker, *Aust. J. Phys.* **39**, 633 (1986); W. Eberhardt, E. W. Plummer, I.-W. Lyo, R. Carr, and W. K. Ford, *Phys. Rev. Lett.* **58**, 207 (1987).

[3] W. Forst, "Theory of Unimolecular Reactions," Academic Press, New York (1973).

[4] T. Ibuki, K. Okada, K. Saito, and T. Gejo, *J. Electron Spectrosc. Relat. Phenom.* **107**, 39 (2000).

[5] L. Claisen, *Ber. Deutsch. Chem. Gesell. (Berlin)* **25**, 1776 (1892).

[6] Y. Kawasaki, A. Fujii, Y. Nakano, S. Sakaguchi, and Y. Ishii, *J. Org. Chem.* **64**, 4214 (1999).

(BL8B1)

Study on Dissociation Dynamics of Core-exited Trifluoromethane in the F K-shell Excitation Region using Auger Electron-Photoion-Photoion Coincidence Measurement

Y. Suto [a], H. Yoshida [a], M. Aratake [a], Y. Senba [a], T. Gejo [b], K. Mase [c], and A. Hiraya [a]

[a] *Department of Physical Science, Hiroshima University, Higashi-Hiroshima 739-8526, Japan.*
[b] *UVSOR, Institute for Molecular Science, Okazaki 444-8585, Japan.*
[c] *Photon Factory, Institute of Materials Structure Science, Tsukuba 305-0801, Japan.*

Core-excited molecules are unstable and Auger decay follows rapidly. Auger electrons are emitted with various kinetic energies and as a consequence, various Auger-final states of singly charged ions are produced. When the energy of Auger-final state is higher than the threshold of double ionization, it can be autoionized into doubly charged ion. This dication often dissociate into ion pair by Coulomb repulsion. To elucidate the detail of the dissociation dynamics of core-excited organic molecules, especially those from the dication produced by auto ionization, Auger electron–photoion–photoion coincidence (AEPIPICO) measurements have been applied to CH_3CN [1] and $(CH_3)_2CO$ [2]. In the present study, we have investigated the dissociation dynamics of trifluoromethane (CHF_3) in the F K-Shell excitation region.

Experimental procedure was described elsewhere [3]. Briefly, a double-focusing time-of-flight (TOF) mass spectrometer [4] and a cylindrical-mirror type electron energy analyzer (CMA) [5] were used for the coincidence measurements between energy-selected electrons and fragment ions. A weak electrostatic field (40 V/cm) was applied to the interaction region and as a result, mass resolution ($M/\Delta M$) of the TOF was estimated to be ~30 and electron energy resolution ($E/\Delta E$) of the CMA ~25. Correlations between two ions produced by an autoionization following Auger process are recorded in a fast multiscaler by using the signal of an energy-selected Auger electron as a start signal and the ion signals as multi-stop signals.

After a measurement of the total ion yield curve for CHF_3 at F1s excitation region, we set the photon energy to top of the σ* resonance (691 eV). A typical AEPIPICO 2-D map obtained for the Auger electron energy of 657 eV is shown in Fig.1. Auger-final-state energy (FSE) of 34 eV is calculated by subtracting the electron energy from the initial excitation energy. Horizontal and vertical axes are the flight time of first and second ion, respectively. Various ion pairs such as F^+/CF^+, F^+/CHF^+, F^+/CHF_2^+ and F^+/CH^+ are observed. The slope of the coincidence peak for the ion pair F^+/CHF_2^+ produced by two-body dissociation is –1. The slope of –1 indicates that the initial momenta of two ions produced by dissociation of dication have same amplitude with opposite direction. Fig.2(a) shows a part of AEPIPICO 2-D map at F^+/CF^+ ion pair region in Fig.1. Slope of the coincidence peak is estimated to be not –1 but about –0.6. This implies a sequential dissociation of the parent dication CHF_3^{2+}. A plausible dissociation mechanism to form this ion pair is considered as follows.

$$CHF_3^{2+}\ (FSE=34eV) \rightarrow F^+ + CHF_2^+ \rightarrow F^+ + CF^+ + H + F\ (or\ HF)\ \ldots\ (1)$$

For this process, slope of the coincidence peak is calculated to be -0.63. The value is in good agreement with the experimental one. Fig.2(b) shows the same part of AEPIPICO 2-D map as Fig.2(a), but obtained for FSE of 59

eV. The slope of this peak is almost –1. The dissociation mechanism is considered as follows.

$$CHF_3^{2+}\ (FSE=59eV) \rightarrow CF_2^{2+} + H + F\ (or\ HF) \rightarrow F^+ + CF^+ + H + F\ (\ or\ HF)\ \ldots\ (2)$$

These observations reveal, for the first time, different dissociation mechanisms for different dicationic states having different Auger-final-state energy.

References

[1] Y. Senba *et al.*, UVSOR Activity Report 2000, 28 (2001) 84.
[2] H.Yoshida *et al.*, UVSOR Activity Report 2000, 28 (2001) 88.
[3] Y. Senba *et al.*, to be published.
[4] A. Hiraya *et al.*, Journal of Electron spectroscopy and related phenomena 101-103 (1999) 1025.
[5] T. Gejo *et al.*, UVSOR Activity Report 1999, 27 (2000) 68.

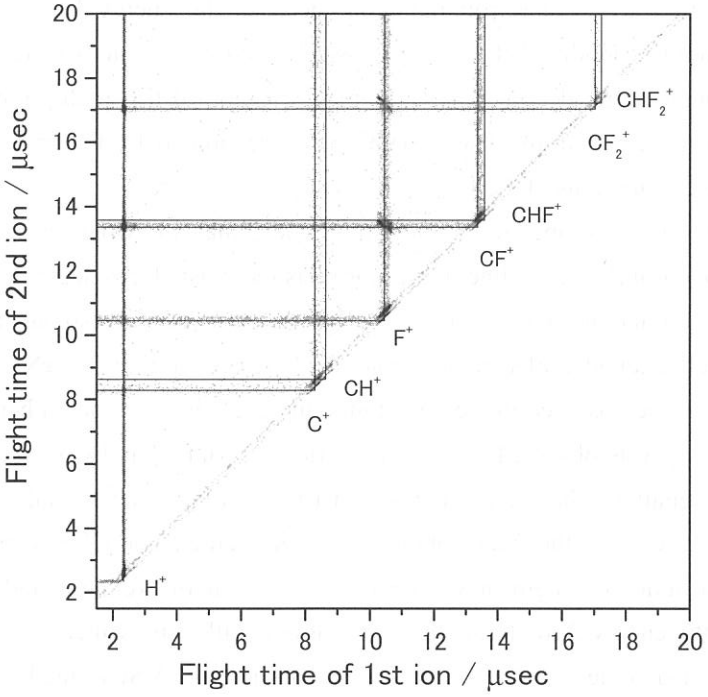

Fig.1. AEPIPICO spectrum obtained for the F1s to σ* (691eV) and for Auger electron energy of 657eV. (FSE=34eV)

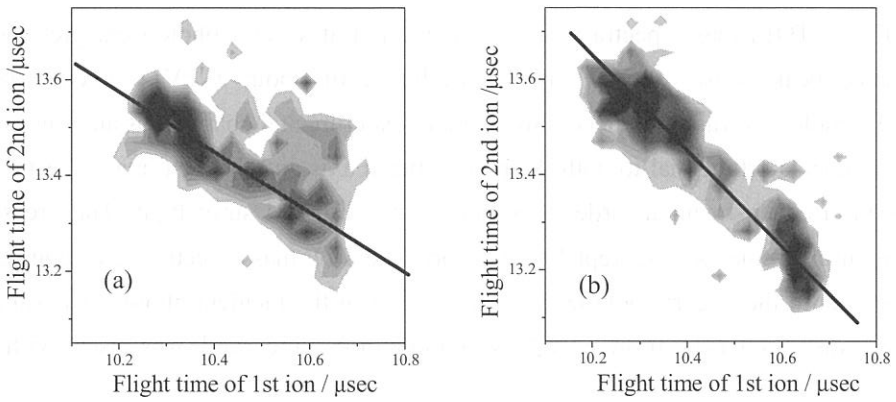

Fig.2. Part of AEPIPICO 2-D maps at F^+/CF^+ ion pair region measured with the final state energy of (a) 34 and (b) 59eV. Reference lines are also shown, which slopes are calculated to be (a) –0.63 and (b) –1.

(BL8B1)

Fragmentation of the C *K*-shell excited CF_3CN molecule studied by angle-resolved TOF mass spectroscopy: Vibrational modes acting as an internal energy reservoir

Shuichiro TANIMOTO, Kazumasa OKADA, Toshio IBUKI,[a] Ko SAITO, and Tatsuo GEJO[b]

Department of Chemistry, Hiroshima University, Higashi-Hiroshima 739-8526

[a] *Kyoto University of Education, Kyoto 612-8522*

[b] *Institute for Molecular Science, Okazaki 444-8585*

Inner-shell electrons of the atom in a specific chemical environment of a molecule can be selectivity excited with a tunable soft x-ray synchrotron radiation, because the energy levels of the inner-shell electrons differ from one atom to another. When the inner-shell electron is photoexcited, a multiply ionized molecule is produced through Auger decays. The Coulomb explosion of this multiply charged molecular ion follows the loss of bonding electrons. The dynamics can be probed by the measurement of mass, angular, and kinetic energy distributions of the fragment ions.

Trifluoroacetonitrile (CF_3CN) is one of the intriguing molecules in two respects. Firstly, we can selectively excite a specific atom (F, N, or either C). Fluorine is the most electronegative atom and induces the largest chemical shift around it in the molecule. Secondly, we can investigate the fragmentation dynamics of the inner-shell excited molecule noticing the linearity of the C–C≡N skeleton. Whether anisotropic fragmentation can be observed in the polyatomic molecule is our concern here. In our previous study [1], a strong anisotropy was observed for the energetic CF_3^+, CF_2^+, and CN^+ fragment ions at the $\pi_{CN}^* \leftarrow$ N(1s) resonance excitation. That is, the Π–Σ symmetry transition basically holds. This report gives an outline of our subsequent work on the fragmentation of the *K*-shell excited CF_3CN molecule. We show that the kinetic energy distribution of fragment ions depends on the site of excitation and the fragmentation competes with intramolecular energy flow. The detailed discussion will be presented elsewhere [2].

The experiments were performed on the beamline BL8B1 at the UVSOR facility. Photoabsorption spectrum was observed at room temperature in the C *K*-shell region with the energy resolution $E/\Delta E$ better than 2000. The experimental setup, procedure, and the obtained photoabsorption spectrum have been given in Ref. [3], and we do not repeat here.

The time-of-flight (TOF) mass spectra were also measured at several photon energies including the prominent resonance peaks observed. An energy resolution of about 1 eV was employed for the measurement. The sample gas was introduced into the main experimental chamber as an effusive molecular beam through a gas nozzle orthogonal to both the photon beam axis and the TOF mass spectrometer tube. An Al filter was inserted upstream in order to suppress the scattered stray light. The pressures in the chamber during the measurements were kept 1×10^{-5} Torr. The TOF mass spectra were acquired at 0° and 90° angles with respect to the linearly polarized electric vector of the incident photon. The sample gas for the present study was purchased from SynQuest Laboratories, Inc. and was used without further purification.

The mass spectral profiles of CN^+, CF_2^+, and CF_3^+ peaks were reproduced by the fitting method developed by Saito and Suzuki [4] to obtain the anisotropy β parameters and kinetic energy distributions. The kinetic energies and the β parameters for the components were determined so as to minimize the

difference between the experimental data and the calculated profile. Figure 1 shows the derived kinetic energy distributions of the CN^+, CF_2^+, and CF_3^+ fragment ions generated at the $C_N(1s)$ and $C_F(1s)$ excitations into the π^*_{CN} level. The kinetic energy distribution of CN^+ was expressed well by a Gaussian function with the maximum at KE ~ 2.7 eV, while those of CF_2^+ and CF_3^+ were split into two components: One is a sharp component with a maximum around 0.1 eV and another is a broad distribution with a maximum at 1.3 and 1.1 eV for the CF_2^+ and CF_3^+ ions, respectively. These high kinetic energies are interpreted by a simple relation of $M(CN^+)/M(CF_n^+) \times 2.7 = 1.4$ and 1.0 eV for CF_2^+ and CF_3^+, respectively, where $M(CN^+)/M(CF_n^+)$ is the mass ratio between the CN^+ and CF_n^+ fragment ions. That is, the axial-recoil approximation is valid for the production of the energetic CN^+ and CF_n^+ fragment ions.

The kinetic energy distributions at the $C_F(1s)$ excitation are as wide as those at the $C_N(1s)$ excitation. We cannot see, however, low kinetic energy components for the CF_2^+ and CF_3^+ fragment ions. A dependence of the kinetic energy distribution of the fragment ions on the site-specific excitation is observed for the first time. That is, fragmentation into the CF_n^+ ions following the $C_N(1s)$ excitation competes with the intramolecular energy flow from the initially excited C_N atom to the CF_3 group. We can claim that most of the CF_3^+ ions are formed with kinetic energies and a part of CF_3^+ (about 20 %) would be produced after energy redistribution through the C–C≡N skeleton into the vibrational modes within the CF_3 group. When a $C_F(1s)$ electron of the CF_3 group is initially excited, energy flow from the CF_3 group to the terminal N atom would occur. However, the CN group is not an effective energy reservoir because it has only one vibrational mode, and thus at any excitation mode the CN^+ fragment ion does not have a small kinetic energy component. The CF_3 group acts as an internal energy reservoir.

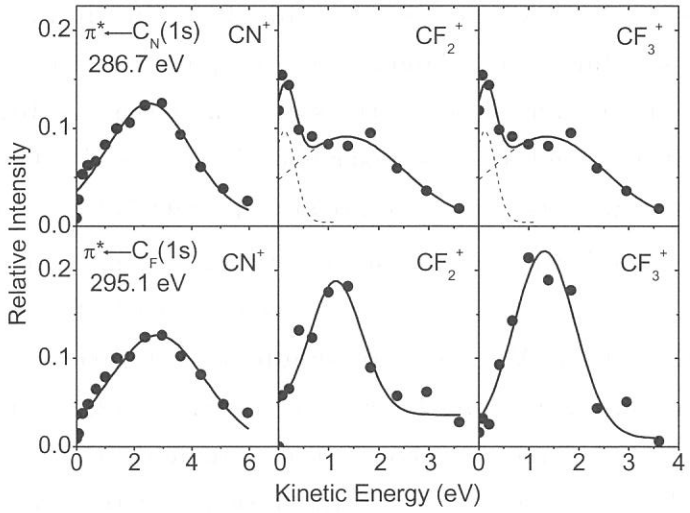

Fig. 1: Kinetic energy distributions of the CN^+, CF_2^+, and CF_3^+ fragment ions generated at the $C_N(1s)$ and $C_F(1s)$ excitations into the π^*_{CN} level.

References

[1] T. Ibuki, K. Okada, T. Gejo, and K. Saito, *Chem. Phys. Lett.* **328**, 147 (2000).

[2] T. Ibuki, K. Okada, S. Tanimoto, K. Saito, and T. Gejo, *J. Electron Spectrosc. Relat. Phenom.*, in press.

[3] K. Okada, S. Tanimoto, T. Ibuki, K. Saito, and T. Gejo, *Chem. Lett.*, 1046 (2001).

[4] N. Saito and I. H. Suzuki, *Int. J. Mass Spectrom. Ion Processes* **82**, 61 (1988).

(BL8B1)

Ultra-fast Dissociation of Core-exited Trifluoromethane in the C K-shell Excitation Region

H. Yoshida [a], Y. Suto [a], M. Morita [a], Y. Senba [a], T. Gejo [b], K. Mase [c], and A. Hiraya [a]

[a] *Department of Physical Science, Hiroshima University, Higashi-Hiroshima 739-8526, Japan.*

[b] *UVSOR, Institute for Molecular Science, Okazaki 444-8585, Japan.*

[c] *Photon Factory, Institute of Materials Structure Science, Tsukuba 305-0801, Japan.*

Core-excited species are unstable and decay processes follow rapidly. The most dominant decay process is resonant Auger electron emission. In some case, the nuclear motion is so fast that dissociation takes place on the same scale as Auger electron emission. Such dissociation in core-excited states is termed "ultra-fast dissociation" and its time scale is considered to be several femtoseconds. It was observed at first for HBr at the Br3d$\rightarrow\sigma^*$ excitation by detecting the atomic Auger emission from the core-excited fragment Br^* [1]. The electronic decay from the core-excited fragment was also observed for CH_2F_2, CHF_3, and CF_4 at the C1s$\rightarrow\sigma^*$ excitation [2]. Those were tentatively assigned to the electron emission from C^* or CF^*. To elucidate the detail of the ultra-fast dissociation processes for CHF_3, Auger electron–photoion coincidence (AEPICO) measurements have been carried out at the soft x-ray beamline BL8B1.

The experimental procedure was described elsewhere [3]. The resonant Auger spectrum following the C1s$\rightarrow\sigma^*$ excitation ($h\nu$=294.7eV) is shown in Fig.1. Horizontal axis is indicated as a scale of Auger-final-state energy (FSE). Spectator-type Auger transitions are observed around 40 and 60 eV, while participant-type around 20 eV. The weak shoulder structure observed at 26 eV is ascribed to the Auger transition from the fragment [2]. Coincidence spectra between energy-selected Auger electrons and fragment ions were measured for various Auger-final-state energies. When the FSE is set to 17 eV, CF_3^+, CF_2^+, and CF^+, which would be produced from the participant-type molecular Auger-final states, are observed in Fig.2(a). On the other hand, only CF^+ is appeared in Fig.2(b) when the FSE is set to 26 eV. This is a clear evidence for the Auger decay from not C^* but CF^* fragments. Such a considerable enhancement for CF^+ yield can not observed for the other core-excited states, for instance, C1s$\rightarrow$3p. We, thus, conclude that after C1s$\rightarrow\sigma^*$ excitation in CHF_3, the ultra-fast dissociation (1) and consequent Auger decay of the fragment (2), as described bellow, take place in competition with the resonant Auger decay within several femtoseconds.

$$CHF_3^*(C1s^{-1}\,\sigma^*) \rightarrow CF^*(C1s^{-1}\sigma^*) + H + F + F \quad (1)$$
$$\rightarrow CF^+ + e^- \quad (2)$$

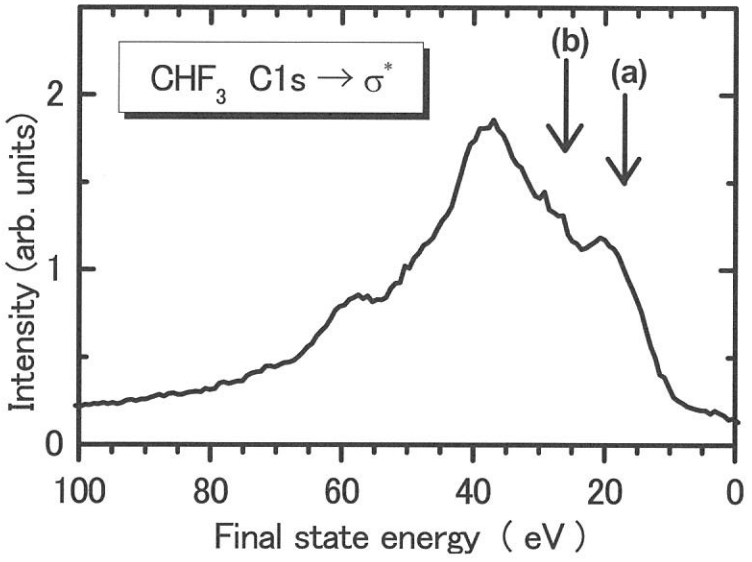

Fig.1 Auger electron spectrum for CHF_3 at C1s→σ^* excitation

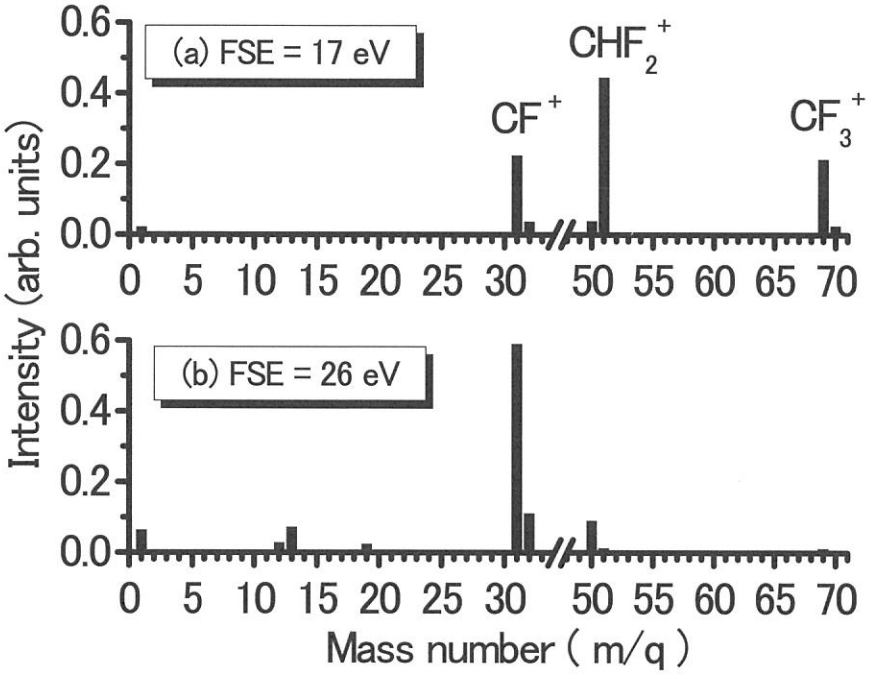

Fig.2 AEPICO spectrum for CHF_3 at C1s→σ^* excitation

References

[1] P. Morin and I. Nenner, Phys. Rev. Lett., 56 (1986) 1913.

[2] K. Ueda et al., J. Electron Spectrosc. Relat. Phenom., 79 (1996) 441.

[3] Y. Senba et al., to be published.